Cross flow over two heated cylinders in tandem arrangements at subcritical Reynolds number using large eddy simulations

Imran Afgan, Yacine Kahil, Sofiane Benhamadouche, Mohamed Ali, Ahmed Alkaabi, Abdallah Sofiane Berrouk, Pierre Sagaut

Cross flow over two heated cylinders in tandem arrangements at subcritical Reynolds number using large eddy simulations

Imran Afgan [a,b,f,*], Yacine Kahil [c,d], Sofiane Benhamadouche [e], Mohamed Ali [a,f], Ahmed Alkaabi [a,f], Abdallah Sofiane Berrouk [a,g], Pierre Sagaut [h]

[a] College of Engineering, Khalifa University of Science and Technology, PO BOX 127788, Abu Dhabi, United Arab Emirates
[b] Department of Mechanical, Aerospace, and Civil Engineering, School of Engineering, University of Manchester, M13 9PL, UK
[c] Science and Technology Faculty, Tissemsilt University, 38000 Tissemsilt, Algeria
[d] Applied Mechanics Laboratory, University of Sciences & Technology Mohamed Boudiaf, 31000 Oran, Algeria
[e] Electricité de France - R&D Division, Fluid Mechanics Energy and Environment Dept. 6, Quai Watier, 78401 Chatou Cedex, France
[f] Emirates Nuclear Technology Center, Khalifa University of Science and Technology, PO BOX 127788, Abu Dhabi, United Arab Emirates
[g] Center for Catalysis and Separation (CeCaS), Khalifa University of Science and Technology, PO BOX 127788, Abu Dhabi, United Arab Emirates
[h] Aix-Marseille University, CNRS, Centrale Marseille, M2P2 Marseille, France

ARTICLE INFO

Keywords:
Large eddy simulation
Heat transfer
Forced convection
Nusselt number
Tandem cylinders
Vortex shedding

ABSTRACT

This study analyses the heat transfer and flow characteristics of cross-flow over two heated infinite cylinders in a tandem (in-line) configuration. Non-isothermal Large Eddy Simulations (LES) using the dynamic Smagorinsky model were conducted at a fixed Reynolds number of 3,000 (based on the free stream velocity and the cylinder diameter). A range of cylinder gap ratios ($1.0 \leq L/D \leq 5.0$) was investigated (in increments of 0.25) with two different Prandtl numbers $Pr = 0.1$ and 1.0. Results show that the flow structures vary according to the order of the patterns: (i) Extended body regime: without attachment for low L/D (1.0 –1.25) where cylinders behave as a single bluff body with top–bottom vortex shedding, (ii) Shear layer reattachment regime: with reattachment for moderate L/D (1.5 –3.75) where the detached shear layer from the upstream cylinder reattaches to the downstream cylinder, and (iii) Co-shedding regime: for high gap ratios ($3.75 \leq L/D \leq 5.0$) a phenomenon called "jumping", where the two cylinders behave as isolated bluff bodies. Furthermore, it was observed that the average Nusselt number of both cylinders experience a drastic variation at a critical spacing ratio (between $3.75 \leq L/D \leq 4.0$). For $L/D \leq 3.0$, the average Nusselt number of the upstream cylinder was found to be higher than that of the downstream one. However, for spacing ratios $L/D > 3.0$, the average Nusselt number was similar for both cylinders. For the downstream cylinder, the maximum Nusselt number was located at the separation angle and was found to be independent of the spacing ratio.

1. Introduction

Fluid-elastic instabilities are a major concern for heat exchangers and steam generators for both conventional coal and nuclear power plants. Such heat exchangers are designed with tens of hundreds of tubes that operate under cross-flow, axial-flow, or mixed-flow directions. In such complex flows, the fluid excitation forces lead to severe vibrations causing extensive irreparable damage to the tubes. Cylinder clusters, especially in cross-flow, have periodic vortex shedding which leads to added forced vibrations. If these vibrations are close to the natural frequency of cylinders, the result could lead to catastrophic failure of the structure. The proximity and wake interaction of such configurations has thus received a lot of attention over the last few decades, especially cross-flow over multiple cylinders in a side-by-side arrangement and flow through arrays of multiple cylinder clusters. A phenomenon that is quite common in such configurations is the flow-biased bi-stability as reported extensively in the past, see (Afgan et al., 2011; Afgan, 2007; Benhamadouche et al., 2005, Alam et al., 2003; Igarashi, 1981; Sumner, 2010; Parezanović and Cadot, 2012; Parezanović et al., 2015; Alameri and Alkaabi, 2020; Kim et al., 2019; Iacovides et al., 2014). The strong confinement effects of densely packed tubes cause the flow to become biased towards one side. Afgan et al. 2011 was the first to document that the vortex shedding in such configurations is always out of phase from each other, however, if the shedding from any two side-by-side cylinders

* Corresponding author.
E-mail addresses: imran.afgan@ku.ac.ae, imran.afgan@manchester.ac.uk (I. Afgan).

becomes in-phase, a flow flip-over occurs which causes the flow to become biased towards the opposite side; a phenomenon called bi-stability. Such behaviour is not only common in large arrays of cylinders but can also be observed for multiple cylinders in cross-flow arrangement, see Kahil et al., 2019 and Benhamadouche et al. 2020 for further details. For such cylinder configurations with varying pitch-to-diameter ratios there can be four different types of interferences; proximity interference, wake interference, combination of proximity and wake interference, and weak interference (Zdravkovich, 2003, 1977). Furthermore, much like varying gap ratios in a side-by-side arrangement can lead to different flow regimes, the inline gap ratios can also lead to different wake interference effects. Thus, to better understand the flow and heat transfer behaviour in inline cylinders, which are fundamental to the understanding of flow through arrays of cylinder clusters, the current paper deals with two tandem in-line cylinders with varying pitch-to-gap ratios.

The flow over two tandem cylinders is classified into three main regimes according to the spacing ratio L/D, where D is the cylinder diameter and L is the center-to-center distance. Early experimental investigations conducted by (Igarashi, 1984, 1981; Zdravkovich, 1987) identified different regimes and boundaries of these regimens according to the Reynolds number and the spacing ratios. The first regime is the extended body regime with a spacing ratio of $1.0 \leq L/D \leq 1.8$; the shear layers of the upstream cylinder do not reattach to the downstream cylinder as it encloses it. Therefore, the vortex shedding observed behind the downstream cylinder is in fact created by the upstream and its frequency is affected by the presence of the downstream cylinder. The second regime occurs for $1.8 \leq L/D \leq 3.8$ where the separated shear layer of the upstream cylinder reattaches to the downstream cylinder. The vortex shedding of the downstream cylinder is then affected by the presence of the upstream. Depending on the spacing ratio, this reattachment regime can be divided into two sub-regimes depending on the reattachment location on the downstream cylinder: front or back side reattachment. For spacing ratio $L/D > 3.8$, the separated shear layers around the upstream cylinder are rolled and generate shaped vortex in front of the downstream cylinder. In this co-shedding regime, vortex shedding is created for both cylinders. What is noteworthy here is that this phenomena happens once the critical step between the two cylinders (L/D 3.8) is exceeded (Alam et al., 2003; Igarashi, 1981; Kitagawa and Ohta, 2008; Ljungkrona et al., 1991; Ljungkrona and Sundén, 1993). (Sumner, 2010) states that it is necessary to consider the extrusion ratio (aspect ratio $AR = L_z/D$) which must be high enough to represent the three-dimensionality of the flow. The most important parameters that dictate the behaviour of the flow in this case are the longitudinal spacing ratios between the cylinder centres and the Reynolds number.

Many researchers studied the flow regimes at low Reynolds numbers. (Mittal et al., 1997) used finite element method (FEM) to study the two-dimensional (2D) flow past two tandem cylinders at Reynolds numbers $Re = 100$ and $1,000$ for spacing ratios (L/D) of 2.5 and 5.5. Results showed a strong dependency of the flow on the Re number. (Jester and Kallinderis, 2003) used FEM coupled with a dynamic mesh to study the flow around tandem cylinders for the Re number range of 80 to $1,000$. simulations allowed were able to reproduce some flow physics features reported experimentally such as bi-stable biased gap flow. (Carmo et al., 2010a, 2010b) investigated the effect of the three-dimensional secondary instabilities on the shedding regime. Numerical simulations were conducted for the Re range of 80 to 500 and spacing ratios between 1.2 and 10. Results showed that for low spacing ratios, the downstream cylinder had a stabilizing effect on the flow and the three-dimensional structures were delayed. However, for high spacing ratios, the three-dimensional structures appeared earlier than the case of a single cylinder, and hence, the downstream cylinder destabilized the flow. Special attention was given to the phase lag between the vortex shedding from the upstream and downstream cylinder by (Alam, 2016). The authors used two-dimensional numerical simulations at a Re number of 200 to study the dependency of the phase lag on the spacing ratio, fluctuation lift, and the Strouhal number.

For high Reynolds numbers (9.7×10^3 to 6.5×10^4), (Alam, 2014) conducted a series of experimental measurements of Strouhal number, fluctuating lift, and drag of a circular cylinder in the wake of an identical one. The spacing ratios between the cylinders varied from 1.1 to 4.5. Based on the results of the measurements, a flow structure map for different Reynolds numbers and spacing ratios was derived. A bi-stable regime was identified between the reattachment and co-shedding regime where both flows occur intermittently. This flow map was later extended by (Wong et al., 2014) for two cylinders in a staggered configuration with different angles and spacing ratios between the inflow and the center-to-center line. Recently, (Zhou et al., 2019) investigated the flow physics around two stationary cylinders at a subcritical Reynolds number of $1,000$ using large eddy simulations. They studied the effect of the spacing ratios (1.25 to 6) on the fluctuating aerodynamic forces and the flow structures; similar regimes to those of (Igarashi, 1981; Zdravkovich, 1987) were identified. The boundaries between different regimes were distinguished by the wake behaviour and variation of different flow parameters. At the boundary between the overshoot (single body) and reattachment flow regimes, wake recirculation and Strouhal number drop, phase lag, fluctuating lift, and drag jump were reported. However, the transition from reattachment flow to a co-shedding regime was reported to be characterized by a drop of wake recirculation and an increase of other parameters.

To study the effect of the different flow regimes on the heat transfer characteristics, numerous studies were conducted considering heated tandem cylinders. (Mahír and Altaç, 2008) conducted 2D numerical simulations to study the convective heat transfer in flow around two tandem cylinders at low Reynolds number (100) and for spacing ratios (L/D) from 2 to 10. For $L/D > 4$, results showed that the mean Nusselt number of the upstream cylinder approached that of a single cylinder and was found to be 25% higher than that of the downstream cylinder. (Harimi and Saghafian, 2012) used an overset method to study the effect of spacing ratio, Reynolds number, and Prandtl number (Pr)on the forced convection heat transfer around tandem cylinders. The local Nusselt number was reported to be affected by the development of the boundary layer, flow separation, and vortex shedding. (Zafar and Alam, 2018) studied the flow and heat transfer of a circular cylinder submerged in the wake of a smaller one. They conducted numerical simulations with forced convection at a Re number of 200, and L/D of 5.5, with varying diameter ratios (0.15 to 1). The authors reported that the heat transfer enhancement for the downstream cylinder was found to be sensitive to the wake strength of the upstream cylinder and the flow regime (impingement, reattachment, or co-shedding). (Abed and Afgan, 2017) studied a wide range of configurations of in-line heated cylinders with a variety of Reynolds Average Navier Stokes (RANS) turbulence models at a moderate Reynolds number of $41,000$. The main aim of the study was to look at the flow bi-stability and the difference in the flow physics between the square and non-square cylinder arrangements. For high Reynolds number, (Dhiman et al., 2017b) experimentally investigated the convective heat transfer in cross-flow past tandem cylinders at Re from 1.1×10^4 to 6.2×10^4 and L/D from 1.2 to 4. The local Nusselt number at the cylinder surface varies according to the flow regime. Correlations for averaged Nusselt number were developed for different segments of the cylinders (impingement, re-attachment, and separation zone) as a function of Re, Pr, and L/D.

Some of the notable studies related to flow and heat transfer around tandem cylinders are given in Table 1. It can be observed that most of the studies considering the flow and heat transfer from tandem cylinders are at low Reynolds numbers and only a few consider the subcritical range of Re, in particular there is a lack of heat transfer data which is very important from the applications point of view. It is thus of great importance to develop a detailed understanding of not just the flow field but also the heat transfer characteristics at a critical Re range. This will aid in a better understanding of the physics behind multiple cylinders

Table 1
Literature review for tandem cylinders: flow and heat transfer. (*Re*: Reynolds number, *Pr*: Prandtl number, *Nu*: Nusselt number, *Ri*: Richardson number, Exp: experimental study).

Study	Mode/ *Re* /*Pr*	Configuration	Measurements
(Ishigai et al., 1972)	Exp/1, 500 −15,000	$1.0 \leq L/D \leq 5.0$	*St*, C_p
(Zdravkovich, 1977)	Exp/60,000	$2.5 \leq L/D \leq 7.0$	C_D, C_p
(Igarashi, 1984, 1981)	Exp/8, 700 −52,000	$1.0 \leq L/D \leq 5.0$	C_D, C_p, $C_p{}'$, *St*
(Moriya et al., 1983)	Exp/ 90,000	$2.0 \leq L/D \leq 5.0$	C_D, C_p, $C_p{}'$, *St*
(Huhe-Aode et al., 1985)	Exp/100 −1, 000	$1.5 \leq L/D \leq 10.0$	*St*
(Ljungkrona et al., 1991; Ljungkrona and Sundén, 1993)	Exp/ =	$1.25 \leq L/D \leq 4.0$	C_p, $C_p{}'$, *St*
(Mittal et al., 1997)	Laminar 2D/ 100, 1,000	$2.5 \leq L/D \leq 5.5$	C_D, C_L, *St*
(Moriya et al., 2001)	Exp/65,000	$2.0 \leq L/D \leq 5.0$	C_D, C_p, $C_D{}'$, $C_L{}'$, St
(Alam et al., 2003)	Exp/65,000	$1.1 \leq L/D \leq 9.0$	C_p, *St*
(Jester and Kallinderis, 2003)	Laminar 2D/ 80, 1,000	$1.1 \leq L/D \leq 9.0$	C_D, C_L, *St*
(Mahír and Altaç, 2008)	Laminar 2D/ 100,200/0.7	$2.0 \leq L/D \leq 10.0$	C_D, C_L, *St*, *Nu*
(Kitagawa and Ohta, 2008)	LES/22,000	$2.0 \leq L/D \leq 5.0$	C_D, C_p, $C_p{}'$, *St*
(Carmo et al., 2010a, 2010b)	Num 2D&3D/ $Re \leq 500$	$1.2 \leq L/D \leq 10.0$	C_D, C_L, second instability
(Sumner, 2010)	Review	–	Structures interaction
(Dehkordi et al., 2011)	$k-\omega$ 2D/100, 200, 22,000	$2.0 \leq L/D \leq 4.0$	C_D, C_L, *St*
(Harimi and Saghafian, 2012)	Laminar 2D/ 100 −200	$2.0 \leq L/D \leq 10$	C_D, C_L, *Nu*
(Koda and Lien, 2013)	Num 2D&3D /160 −220	$1.5 \leq L/D \leq 8$	C_D, $C_D{}'$, C_L, $C_L{}'$, *St*
(Alam, 2014)	Exp/0.7 × 10^3 −6.5 × 10^4	$1.1 \leq L/D \leq 4.5$	$C_D{}'$, $C_L{}'$, *St*
(Wong et al., 2014)	Exp/1, 500 −20,000	$1.2 \leq L/D \leq 6.0$	Structures interaction
(Salcedo et al., 2016)	Num 2D/ 200/ 0.744 (-1 ≤ *Ri* ≤ 4)	L/D = 2.0, 3.0, and 5.0	*Nu*, velocity profiles
(Alam, 2016)	Num 2D/200	$2.0 \leq L/D \leq 9.0$	C_D, $C_D{}'$, C_L, $C_L{}'$, C_p, $C_p{}'$, *St*, phase lag
(Dhiman et al., 2017b)	Exp/11, 000 −62,000	$1.2 \leq L/D \leq 4.0$	C_p, *Nu*
(Dhiman et al., 2017a)	$k-kl-\omega$/11, 000 −41,000	$1.2 \leq L/D \leq 4.0$	C_D, C_L, *Nu*, *Nu*′, *St*
(Maduta et al., 2017)	Eddy-resolving RSM /166,000	L/D = 1.435, 3.7	C_p, $C_p{}'$, *TKE*, flow patterns,
(Abed and Afgan, 2017)	*EBRSM*, *SSTk* −ω, standard $k-\varepsilon$, $v2-f$, and *EBk* −ε/41,000	Square and non-square arrangements ($1.2 \leq L/D \leq 5.0$)	C_p, C_D, C_L, *Nu*, *St*
(Zafar and Alam, 2018)	Laminar 2D/ 200/0.71	$L/D \leq 5$ and $0.3 \leq d/D \leq 1.0$(Diameter ratio)	C_D, $C_D{}'$, C_L, $C_L{}'$, *Nu*, *Nu*′
(Zhou et al., 2019)	LES/1,000	$1.2 \leq L/D \leq 6.0$	C_D, $C_D{}'$, C_L, $C_L{}'$, C_p, $C_p{}'$, *St*
(Zafar and Alam, 2020)		$1.0 \leq L/D \leq 5.0$	
(Zafar et al., 2020)	Num 2D/ 100/ 0.7 ($-0 \leq Ri \leq 2$)		C_D, C_L, *Nu*, Reynolds stresses
(U. Ali et al., 2021)	Review	–	Flow structures and heat transfer
(Rastan and Alam, 2021)	Review	–	Flow structures

and large tube bundle arrays for future investigations.

In the current paper, numerical methods are discussed in Section 2. This is followed by the test case description in Section 3 and results and discussions detailed in Section 4. Special attention is given to the jump phenomena and the discussion of underlying flow physics for the tandem cylinders, which is reported in detail in Sections 4.1 to 4.4. Section 4.5 is dedicated to heat transfer characteristic discussions. Conclusions of the present numerical investigation and recommendations for future work are then given in Section 5.

2. Numerical method

The numerical investigations were carried out using the open-source solver Code_Saturne (https://www.code-saturne.org). This in-house solver developed by Électricité de France (EDF) is based on a collocated unstructured finite volume method and has been extensively tested and benchmarked over a variety of heat transfer, thermal hydraulics, and other industrial applications in the past, see (Abed et al., 2021, 2020c,2020a,2020b; Afgan et al., 2011, 2008; Ahmed et al., 2021; Ali et al., 2021a,b; Ali et al., 2022; Benhamadouche et al., 2020; Benhamadouche, 2006; Filippone and Afgan, 2008; Guleren et al., 2010; Nguyen et al., 2020; Revell et al., 2020; Wu et al., 2017). The pressure–velocity coupling is performed using a SIMPLEC algorithm with the (Rhie and Chow, 1983) interpolation to eliminate odd–even oscillations. A detailed description of numerical approaches used in Code_Saturne can be retrieved in (Archambeau et al., 2004; Benhamadouche, 2006; Afgan, 2007, Adobes et al.,2010; Han et al., 2012).

In the current investigation, the flow is considered Newtonian with constant properties (density, viscosity, specific heat, and thermal conductivity). Applying the LES filtering operation, the filtered Navier Stokes equations are written as:

$$\frac{\partial \widetilde{u}_i}{\partial x_i} = 0, \tag{1a}$$

$$\frac{\partial \widetilde{u}_i}{\partial t} + \frac{\partial \widetilde{u}_i \widetilde{u}_j}{\partial x_j} = -\frac{1}{\rho}\frac{\partial \widetilde{p}}{\partial x_i} + \nu \frac{\partial^2 \widetilde{u}_i}{\partial x_j \partial x_j} - \frac{\partial \tau_{ij}}{\partial x_j}. \tag{1b}$$

$$\frac{\partial \widetilde{T}}{\partial t} + \frac{\partial \widetilde{u}_j \widetilde{T}}{\partial x_j} = \frac{\nu}{Pr}\frac{\partial^2 \widetilde{T}}{\partial x_j \partial x_j} - \frac{\partial q_j}{\partial x_j}. \tag{1c}$$

With $\widetilde{u}_i$, $\widetilde{p}$, and $\widetilde{T}$ stand for the filtered velocity components, pressure, and temperature respectively. The dynamic Smagorinsky approach based on Germano identity (Germano et al., 1991) and Lilly (Lilly, 1992) minimization is used to model the sub-grid scale tensor τ_{ij} with a deviatoric part given by:

$$\tau_{ij} - \frac{1}{3}\tau_{kk}\delta_{ij} = -2\nu_t \widetilde{S}_{ij} = -2(C_s \widetilde{\Delta})^2 \|S\| \widetilde{S}_{ij}, \tag{2}$$

Where the filtered strain-rate tensor is given by $\widetilde{S}_{ij} = \frac{1}{2}\left(\frac{\partial \widetilde{u}_i}{\partial x_j} + \frac{\partial \widetilde{u}_j}{\partial x_i}\right)$ and $\|S\| = \sqrt{2\widetilde{S}_{ij}}\widetilde{S}_{ij}$. ν_t is the sub-grid scale viscosity, $\widetilde{\Delta}$ is the filter width, and C_s the dynamic Smagorinsky constant. *Pr* is the molecular Prandtl number which is considered constant for the current simulations. To investigate its effect on the heat transfer properties, two different

Prandtl numbers are considered $Pr = 0.1$ and 1.0. q_j is the sub-grid scale heat flux and is also modelled similar to the sub-grid scale tensor using an eddy-dissipation hypothesis as $q_j = \frac{\nu_L}{Pr_t}\frac{\widetilde{\partial T}}{\partial x_j}$, with Pr_t is the turbulent Prandtl number and its value is $Pr_t = 0.85$.

A fully hexahedral mesh is considered with a local filter width given by $\widetilde{\Delta} = 2V^{1/3}$, where V is the computational cell volume. The dynamic constant C_s was evaluated by applying an explicit filter using only the adjacent (sharing a common face) neighbors of every cell. For the stability of the procedure, the C_s constant was capped between 0 and 0.065 (0.13 for the global constant value, i.e., $2 \times C_s$).

The Adams-Bashforth interpolation was used to estimate the explicit mass flux, hence the three components of the velocity are uncoupled for solving the momentum equations. A 2nd order central difference scheme was used for space and time discretization: Crank-Nicolson in time with linearized convection terms, and 2nd order Adams-Bashforth for the viscous terms. A 1% local blending with 1st order upwind scheme is used (Ferziger and Perić, 2002) to avoid artificial numerical wiggles induced by the pure 2nd order central differencing with large and non-orthogonal control volumes. For non-orthogonal grids, only the orthogonal contributions of the different operators are included in the matrix while the non-orthogonal parts are added to the right-hand side of the transport equations. Therefore, inner iterations are needed for velocity and pressure equations to implicitly reconstruct the gradients.

3. Test cases and computational details

Fig. 1 shows a configuration of two cylinders in tandem ($Re_{D,U_0} = 3,000$) with variable longitudinal spacing ratios between cylinders ($L/D = 1.0 - 1.25 - 1.5 - 1.75 - 2.0 - 2.5 - 3.0 - 3.5 - 3.75 - 4.0 - 5.0$). According to the recommendation of Tamura et al 1998, it is necessary to make the spanwise domain length $L_z/D \geq 1.0$ to achieve good results for the time-mean and variance of the aerodynamic forces on the cylinders. During the benchmark study about turbulent flow past two tandem cylinders, the effect of the spanwise length was studied (UFR 2–12 Test Case - KBwiki (ercoftac.org)). The results showed that the sensitivity of the major characteristics of the flow around the cylinders is marginal for $L_z/D \geq 3.0$ (more details can be retrieved from the project website or (Lockard, 2011)). Moreover, (Afgan et al., 2011) studied the effect of the spanwise extrusion using the auto-correlation of spanwise velocity and found that $L_z/D = 4.0$ is sufficient to produce accurate flow statistics. Therefore, the spanwise domain length was set to $L_z/D = 4.0$ in this study similar to the LES investigations of (Zhou et al., 2019) for tandem cylinders, (Kahil et al., 2019) for an array of four cylinders, and (Afgan et al., 2011) for two side-by-side cylinders. The dimensions of the domain computation were 25D, 20D, and 4D, in streamwise (X), transverse (Y), and spanwise (Z) directions respectively. The upstream length of the domain for all the simulations was set to 10D. At the inlet, a uniform speed (without turbulence) was imposed. The top (Y_{max}) and the bottom (Y_{min}) boundaries were considered symmetric while the periodicity condition was imposed in the spanwise direction. At the outlet, an advective boundary condition is applied for the pressure to avoid the reflection of pressure waves. For the temperature, a uniform Dirichlet temperature field is applied at the inlet and on the cylinder surfaces such as $T = 0$ at the inlet and $T = 1$ at the cylinder surfaces. The mesh shown in Fig. 2 is for the cross-spacing of $L/D = 1.5$ which contains 22 million cells (with a resolution of 256 cells in the spanwise direction).

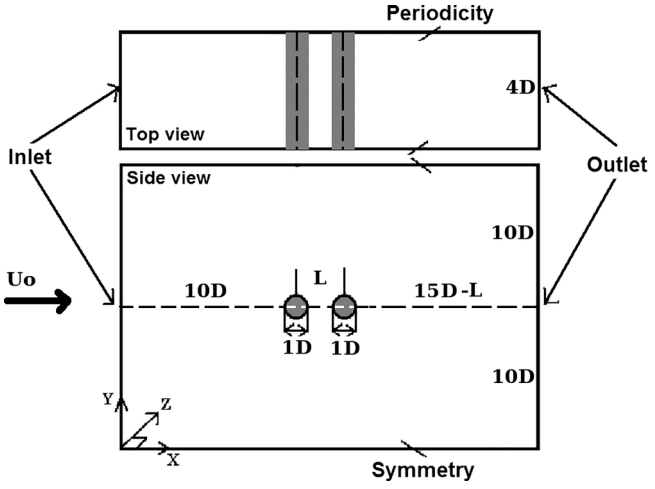

Fig. 1. The computational domain for a single cylinder in XY (side view) and XZ planes (top view).

The dimensionless numerical time ($\Delta t^+ = \Delta t U_0/D$) is set at 0.005, where U_0 is the flow velocity and Δt is the physical value of the time step used for the simulations. This leads to a maximum Courant-Friedrich-Lewy number (CFL) of 0.7 with one passage of the fluid corresponding to about 5,000 time steps. For the configuration of two cylinders in tandem (for the case with spacing $L/D = 1.5$), the calculations were performed on a physical time equal to 810 seconds, which was about 145 vortex shedding cycles for both cylinders. At the end of the simulations, the results were also averaged in space in the periodic direction (Z) to ensure a better statistical convergence.

A dimensionless near-wall resolution around the cylinder surface (0 −360 degrees) in polar coordinates is shown in Fig. 3. It is observed in this figure that the maximum value of the normal distance to the wall ΔR^+ (also ΔY^+ in Cartesian coordinates) does not exceed 1.5 for the upstream cylinder and remains less than 1 for the downstream cylinder; the maximum non-dimensional delta distance in the spanwise (ΔZ^+) is 9.0 for the upstream cylinder. The maximum non-dimensional delta distance in the azimuthal direction (or longitudinal) $\Delta\theta^+$ (also ΔX^+ in Cartesian coordinates) is less than 9.0. However, for the downstream cylinder, both distances are less than 6.0. In the region of the wake cylinders (90 −270 degrees) in the same Fig. 3, we can see that for the upstream cylinder the maximum values of ΔR^+, ΔZ^+, and $\Delta\theta^+$ are equal to 0.3, 2.5, and 2.2, respectively. However, for the downstream cylinder, maximum values are 0.8, 3.0, and 5.0 respectively.

A comprehensive sensitivity study was also conducted based on a single cylinder where domain extrusion and resolution in span-wise direction, sub-grid scale model, and upwind blending were tested. It was observed that there is almost no change in the velocity profile with an increase in the grid resolution and the extrusion length in the span-wise direction. However, the mean solution was found to be very sensitive to the grid refinement in the wall-normal direction. Lack of resolution in the latter case would cause an underprediction of both recirculation length and maximum velocity deficit in the cylinder wake. As a consequence, for all the simulations herein, an extrusion length of 4D and maximum Y^+ close to unity was used. As far as subgrid-scale modelling is concerned, it was found that switching off the sub-grid scale model had drastic effects on both the recirculation length and the velocity profile. The use of the dynamic Smagorinsky LES model with 1% blending yielded a very good match between the numerical predictions and the experimental data of (Parnaudeau et al., 2008) in terms of recirculation length and the wake profile. The use of 1% local blending in the far wake and upstream directions to avoid artificial oscillations was also confirmed not to affect the mean quantities as already shown by (Afgan et al., 2011). Thus, for all the simulations herein, the dynamic LES model with 1% local blending was used.

All simulations were performed using the supercomputer Blue Gene/P (100$TFLOPS$: 10^{14} floating point operations per second). Each simulation was performed using a total of 1,024 or 2,048 processors and each has a wall clock time of 150 hours CPU (central processing unit). This translates to about 12 fluid passages in the computational domain.

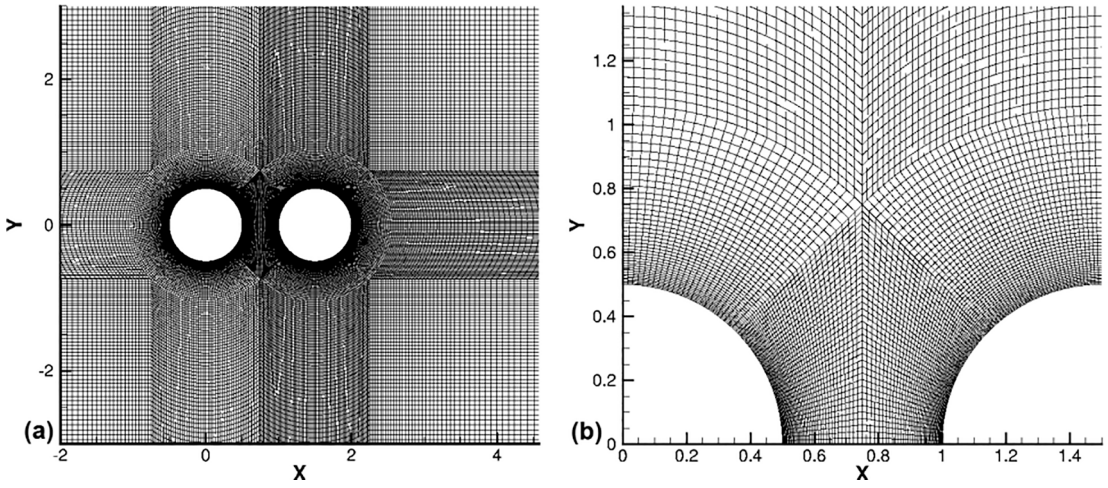

Fig. 2. Computational mesh in XY plane for the two cylinders in tandem configuration with a pitch-to-diameter ratio $L/D = 1.5$. (a) Cross-sectional view. (b) Zoomed view near the cylinder.

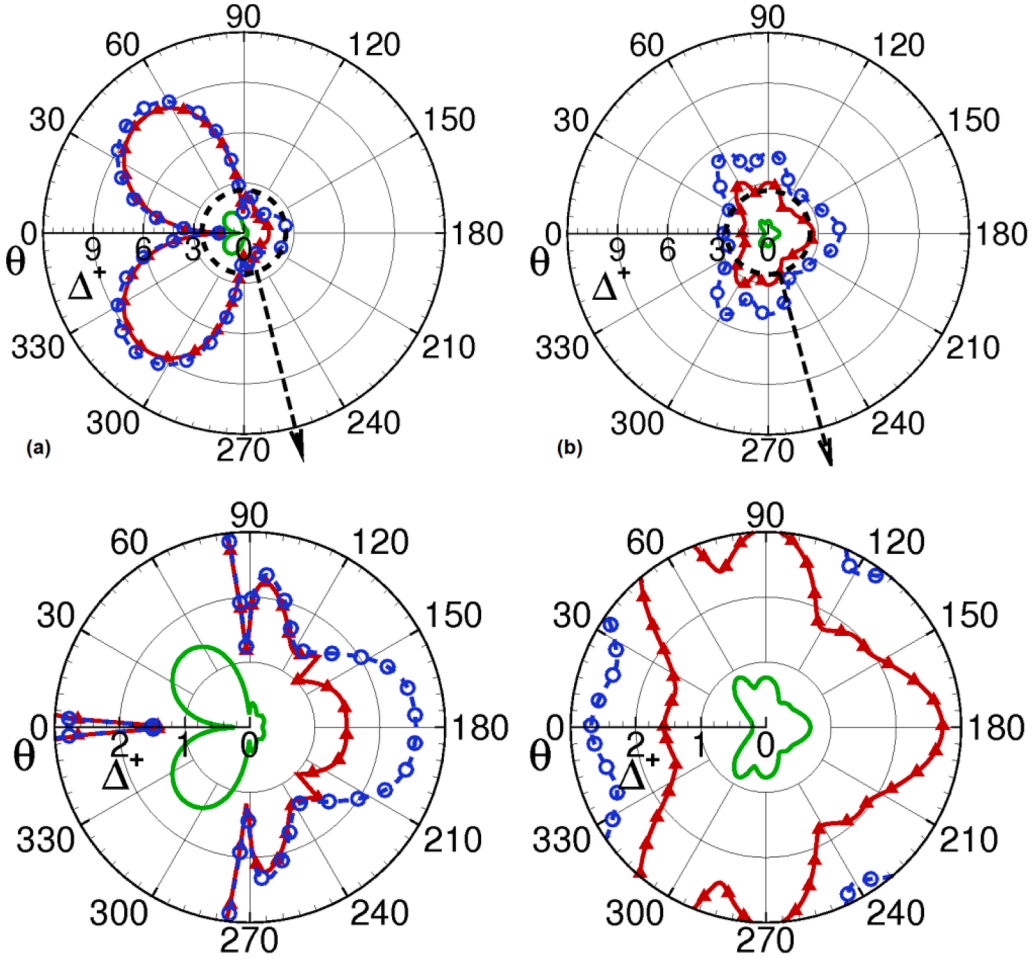

Fig. 3. Non-dimensional wall distances in polar coordinates (top row) and their zooms (bottom row) around cylinder surface for the two cylinders in tandem configurations for pitch to diameter ratio $L/D = 1.5$ at $Re_{D,U_0} = 3{,}000$. (a) Upstream cylinder. (b) Downstream cylinder. – ΔR^+, ∘ ΔZ^+, ▲ $\Delta\theta^+$. (For interpretation of the references to colour in this figure legend, the reader is referred to the web version of this article.)

4. Results and discussion

4.1. Wake topology

For the current simulations, cross-flow over two tandem cylinders with varying L/D ratios (1.0 to 5.0 in increments of 0.25) were simulated at a Re_{D,U_0} number of 3,000. Following the simulations, both the vorticity contours and the isosurface contours of the instantaneous Q-criterion were plotted in a systematic fashion as shown in Fig. 4 below. This figure also shows the comparative flow patterns as suggested by Xu

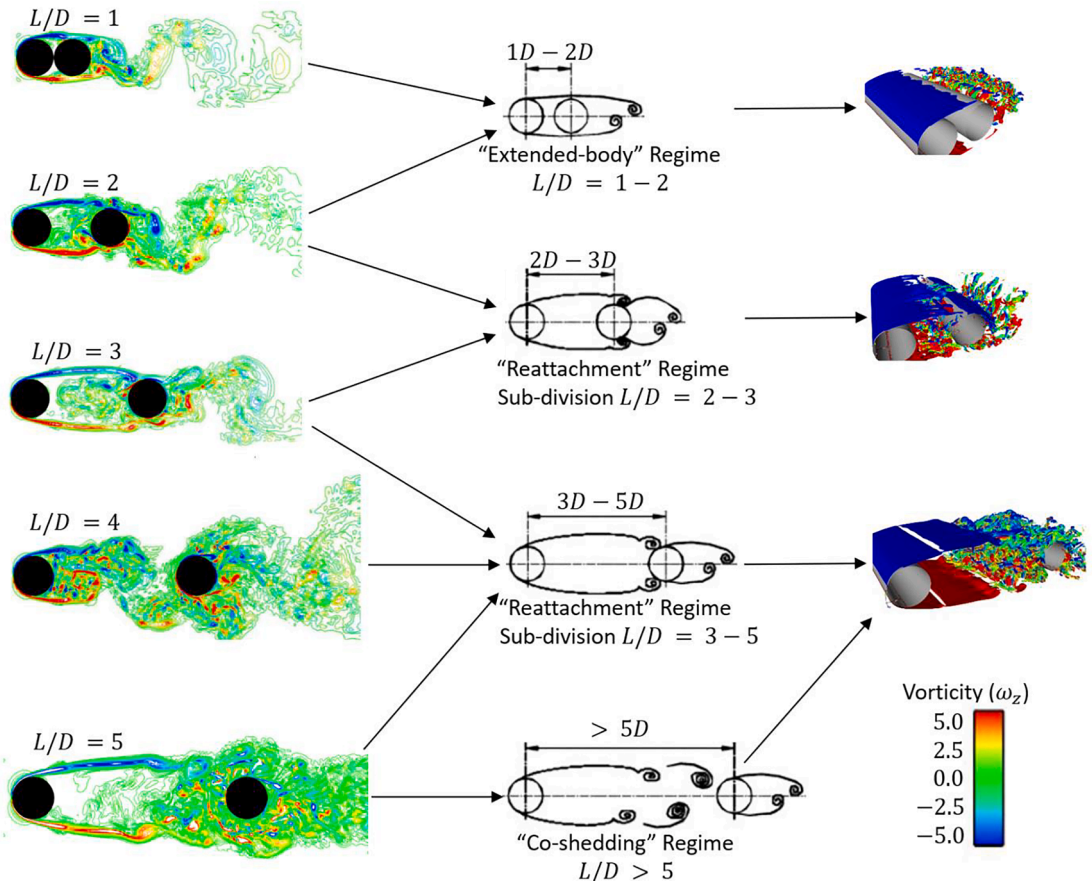

Fig. 4. Comparisons of the vorticity (ω_z) contours (left hand side column) of the current simulations with flow pattern sketches of Xu and Zhou (2004) and Zhou and Yiu (2006) (middle column) and isosurface contours of the instantaneous Q-criterion streamlines of the average velocity field (right hand side column) at various spacing ratios $L/D = 1.0$ to 5.0.

and Zhou (2004) and Zhou and Yiu (2006). As per Zdravkovich (1987), the flow patterns can be classified into three categories. The first regime is the "extended body regime" with a spacing ratio of $1.0 \leq L/D \leq 1.8$ in which the shear layers of the upstream cylinder do not reattach to the downstream cylinder, but rather encloses it. Therefore, the vortex shedding observed behind the downstream cylinder is in fact created by the upstream cylinder and its frequency is affected by the presence of the downstream cylinder. One can clearly see this from the vorticity contours at $L/D = 1$ in Fig. 4.

The second regime "shear layer reattachment regime" occurs for $1.8 \leq L/D \leq 3.8$ where the separated shear layer of the upstream cylinder reattaches to the downstream cylinder. The vortex shedding of the downstream cylinder is then affected by the presence of the upstream. Depending on the spacing ratio, this reattachment regime can be divided into two sub-regimes depending on the reattachment location on the downstream cylinder: "fore-body" or "after-body" reattachment. This is found to be a function of the spacing ratio. As the space ratio is increased, the reattachment location of the upstream cylinders free shear layer, on the downstream cylinder tends to move towards its front. This can clearly be observed from the vorticity plot comparisons of $L/D = 2$ to $L/D = 3$ in Fig. 4. It is also interesting to note here that the vortices or gap eddies as termed by Lin et al., 2002 vary intermittently in terms of their strength, asymmetry and behaviour. As the gap ratio is further increased one observes that the free shear layers of the upstream cylinder no longer reattach on the downstream cylinder. In fact, these are dissipated into smaller vortices or eddies which then come and impact the downstream cylinder. For the current simulations at a Re_{D,U_0} of $3,000$, this flow behaviour was found to be for spacing ratios (L/D) greater than 3.8. Zhou and Yiu (2006) reported this to extend over the range of $2 < L/D < 5$. Zdravkovich, 1987 reported this range to be over $1.8 < L/D < 3.8$. Again, this difference in the inference of the flow regime is due to the difference in Re numbers, as the Re number is increased the range of this "shear layer reattachment regime" increases.

For spacing ratio $L/D > 3.8$, it was observed that the separated free shear layers of the upstream cylinder are rolled into eddies and vortices in front of the downstream cylinder. As the downstream cylinder also sheds its vortices, this flow regime is called "the co-shedding regime", vortex shedding is created for both cylinders. This can clearly be seen from both the vorticity plots and the IsoQ surfaces at $L/D = 5$ in Fig. 4 below. What is noteworthy here is that this phenomena happens once the critical step between the two cylinders (L/D 3.8) is exceeded (Alam et al., 2003; Igarashi, 1981; Kitagawa and Ohta, 2008; Ljungkrona et al., 1991; Ljungkrona and Sundén, 1993). (Sumner, 2010) states that it is necessary to consider the extrusion ratio (aspect ratio $AR = L_z/D$) which must be high enough to represent the three-dimensionality of the flow. The most important parameters that dictate the behaviour of the flow in this case are the longitudinal spacing ratios between the cylinder centres and the Reynolds number.

Fig. 5 shows the streamlines around the two cylinders in tandem for all the spacing ratios $L/D = 1.0$ to 5.0. One can notice that for the case with $L/D = 1.0$ the recirculation behind the downstream cylinder approaches the case of an isolated cylinder. For $L/D = 1.25$, one can see recirculation regions forming behind both the upstream and downstream cylinders; this is because sufficient space is now available for the flow to form local recirculation regions in the inter-cylinder gap. At $L/D = 1.5$, the gap is sufficient for the free shear layer of the upstream cylinder to impinge on and around the downstream cylinder as also observed from the vorticity contours and IsoQ surfaces in Fig. 4.

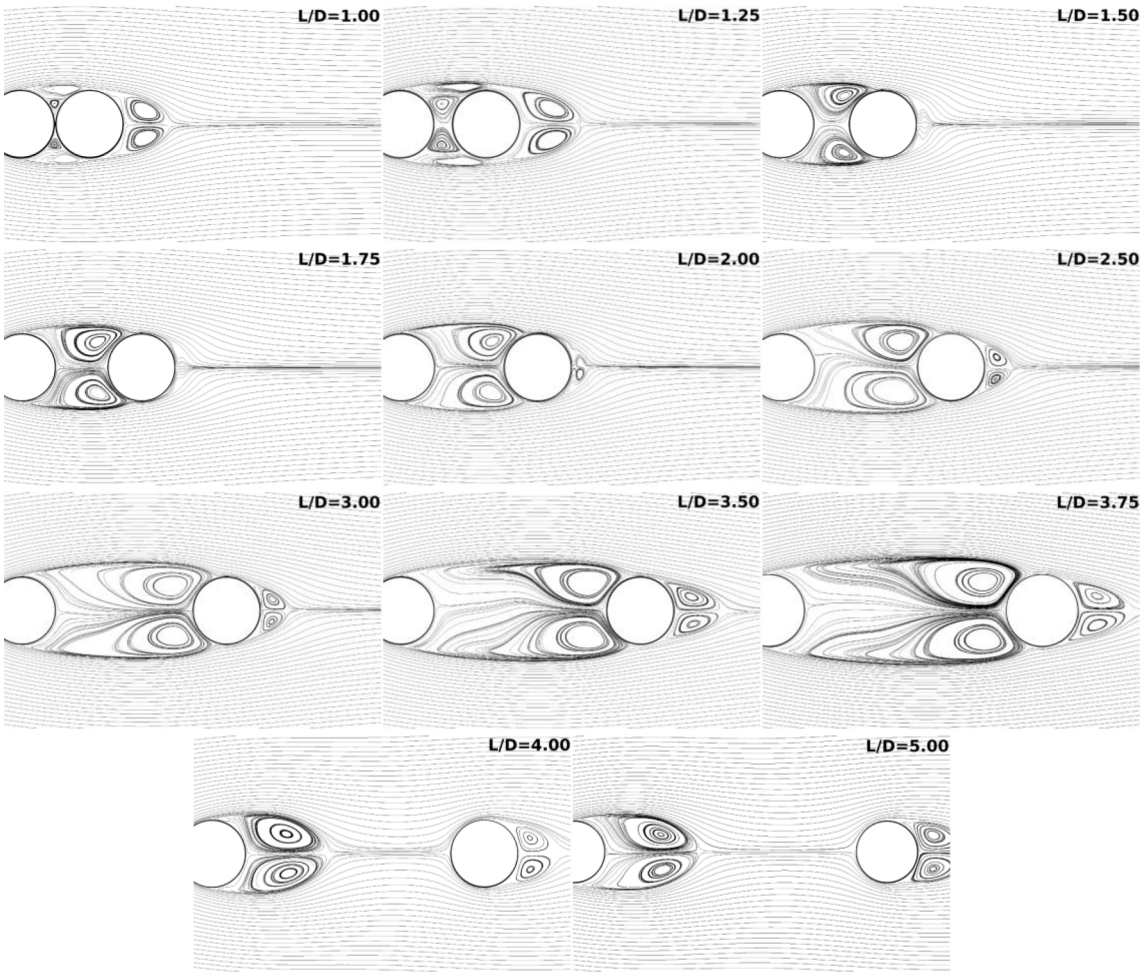

Fig. 5. Streamlines of the average velocity field for various spacing ratios $L/D = 1.0$ to 5.0.

Passing $L/D = 1.5$, a new change in flow behaviour was observed. One notices the absence of a recirculation zone behind the downstream cylinder for this flow regime. In fact, the shear layer separated from the upstream cylinder reattaches the downstream cylinder at or around $\theta \approx 90^0$ and the flow remains attached to the backside of the cylinder. For $L/D = 1.75$, streamlines show the same behaviour as for $L/D = 1.5$. With a further increase in spacing $L/D = 2.0$ to 3.0, the flow regime changes again. For this regime, the separated shear layer of the upstream cylinder is reattached to the downstream cylinder and is separated a second time to form small vortexes in the downstream wake zone.

The flow behaviour mentioned above is the same for all spacing ratios between $L/D = 3.5$ and 3.75, the only difference is the critical re-

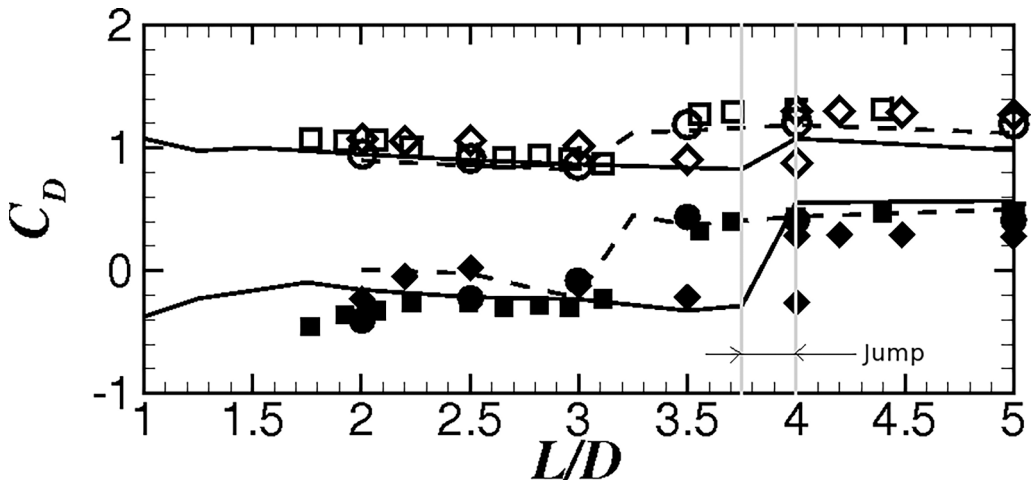

Fig. 6. Mean drag coefficient for the two cylinders in tandem with various spacing ratios $L/D = 1.0$ to 5.0. Open Symbol: upstream cylinder, full symbol: downstream cylinder. −: LES, — : LES (Kitagawa and Ohta, 2008) $Re = 22,000$, ○ and ●: Exp (Ljungkrona et al., 1991) $Re = 20,000$, □ and ■: Exp (Igarashi, 1981) $Re = 35,000$, ◇ et ◆: Exp (Moriya et al., 2001) $Re = 65,000$.

gion where the jump may start to occur. For the spacing ratio of $L/D = 4.0$, the flow behaviour changes for the final time where the so-called zone of instability is exceeded. Here we denote L_{R1} and L_{R2} as recirculation lengths for the upstream and downstream cylinders, respectively. One notices here that the two cylinders have the same behaviour as that of an isolated cylinder but with a difference in the recirculation length (L_{R2}). For spacing $L/D = 5.0$, we remain in the same class, and in addition, the recirculation length L_{R2} of the downstream cylinder is closer to that of the upstream cylinder. However, this is far from reality (L_{R2} L_{R1}) due to the presence of strong turbulence behind the upstream cylinder and which has a great influence on the downstream cylinder.

4.2. Drag, lift and pressure coefficients

The average drag coefficient compared with the space ratio L/D is shown in Fig. 6. As can be seen, the values for $L/D = 2.0 - 3.5$ are in good agreement with experimental data. However, for a small spacing ratio $L/D = 1.0$ to 1.75 there is a lack of experimental data for comparisons and hence only current, numerical results are available. In the literature, a critical step (Jump) is observed for the range of $L/D = 3.25$ to 4.0 as summarized in Table 2. For the current simulations, the critical step was found to be between 3.75 and 4.0; clearly observed from the jump in the mean values of C_D (due to the change of mode as discussed earlier).

For $L/D \leq 3.0$ the variance of the drag coefficient is shown in Fig. 7, where the comparison with existing data shows a good agreement. For the values at $L/D > 3.0$, it is noticed that there is a slight underestimation of $C_D{}'$ for both cylinders. However, the current results are still better than those of (Kitagawa and Ohta, 2008) LES. The difference between current numerical values and the experimental data is actually due to the difference in the Reynolds number; much higher for the experiments.

The variance of the lift coefficient in Fig. 8. It shows a good agreement with experimental data and is substantially better than the numerical results of (Kitagawa and Ohta, 2008). From this figure, one can clearly see the jumping values, which show the flow mode change from $L/D = 3.75$ to 4.0.

Fig. 9a shows a distribution of the mean pressure coefficient around the upstream cylinder where $L/D = 2.0$. The comparisons of the current results with the experience of (Ljungkrona et al., 1991) and the simulation of (Kitagawa and Ohta, 2008) are very close. However, for the experiment of (Moriya et al., 1983), there is a slight difference after the angle $\theta = 90^{\circ}$.

For the downstream cylinder (Fig. 9b), the mean C_p shows a concordance of our results with (Ljungkrona et al., 1991) experiment when $\theta < 80^{\circ}$ and nearly identical to the LES of (Kitagawa and Ohta, 2008). It can also be noticed from this figure that after the angle $\theta = 80^{\circ}$, the current predictions move away from the (Ljungkrona et al., 1991) profiles and they approach the (Moriya et al., 1983) profiles. Same observations can be made for the LES results of (Kitagawa and Ohta, 2008), which are closest to those of (Moriya et al., 1983) even if the Reynolds number is the same as that used by (Ljungkrona et al., 1991).

For Fig. 10a at ($L/D = 3.0$), the distribution of the mean C_p on the upstream cylinder is very close to the results of (Ljungkrona et al., 1991), (Moriya et al., 1983), and the simulations of (Kitagawa and Ohta, 2008).

For the downstream cylinder in Fig. 10b, a good agreement is observed with the reference data. Moreover, for distances $L/D = 2.0$ to 3.0, the same behaviour for the two cylinders is observed. This is because the two configurations are in the lower range where the shear layer of the upstream cylinder reattaches to the downstream cylinder without releasing vortices from the first one.

In comparison with previous profiles for the mean C_p around the upstream cylinder in Fig. 11, one notices a change when approaching the shear layer; this shows a physical change in the flow for this configuration. For a better view of this phenomenon, Figs. 4 and 5 (wake topology) show that we are following the change well and the current results are in good agreement with the experimental data.

Any change on the upstream cylinder has a direct impact on the downstream cylinder, as can be seen in Fig. 10. What is interesting to note is that the peak of the mean C_p changes position as it passes $\theta = 70^{\circ}$ (position re-attachment, $L/D = 2.0$ to 3.0) to $\theta = 0^{\circ}$. We also see that our numerical results coincide well with the experimental data. However, at $\theta = 90^{\circ}$, (Moriya et al., 1983) shows that the mean C_p profile at this angle moves away from the other results.

Cross comparisons of the pressure of the upstream and downstream cylinders (Figs. 9-11) reveal some interesting results. First of all, one notices that for the upstream cylinder the pressure coefficient profile does not vary much when the L/D ratio is changed from 2 to 3. However, at $L/D > 3.8$, there is a marked drop in the C_p coefficient on the back of the upstream cylinder (from around $100 - 180^{0}$). This clearly indicates that after the "jump" there is a release in pressure due to the downstream blockage removal. On the other hand, the C_p profile of the downstream cylinder almost always shows clear differences when the spacing ratio (L/D) is increased from 2 to 3 and 4. Furthermore, one also notices that at $L/D = 4$, the C_p behaviour of the downstream cylinder is now very similar to that of a single cylinder. This indicates, that the free separated shear layer of the upstream cylinder has now broken down into eddies/vortices and is no longer affecting the downstream cylinder as it was for small gap ratios i.e., $2 < L/D < 3$. However, one can see that at $L/D = 4$ the upstream proximity interference is still visible in terms of highly turbulent flow causing a lower (front-back) pressure difference on the downstream cylinder. This is completely the opposite behaviour of what was observed for the range $2 < L/D < 3$ where the separated free shear layer of the upstream cylinder was impacting on the downstream cylinder (either on the "fore-body" or "after-body"). Furthermore, comparing the downstream C_p profiles of the $L/D = 2$ case (Fig. 9) with that of $L/D = 3$ case (Fig. 10) reveals the change in the reattachment location which has now moved forward. Admittedly, both these cases are of the "fore-body" reattachment and for the "after-body" reattachment profiles one has to focus on very small gap ratios (approximately $L/D = 1.25$ to 1.75). Xu and Zhou, 2004 and Zhou and Yiu, 2006 predict this range to be from $2 < L/D < 3$ as their measurements were conducted at much higher *Re* numbers.

Table 2
Critical spacing ratio (***TI***: turbulence intensity of the inflow).

Reference	Type of Study	Reynolds number	Spanwise length	Critical Spacing ratio
(Igarashi, 1981)	Experimental	35,000	–	3.53 – 3.68
(Ljungkrona et al., 1991)	Experimental	20,000	–	$TI = 0\% \rightarrow$ same as (Igarashi, 1981) $TI = 1\% \rightarrow 3.5$ $TI = 1.4\% \rightarrow 2.5$
(Moriya et al., 2001)	Experimental	65,000	–	4.0
(Papaioannou et al., 2006)	Numerical: LES	350 – 1,000	3π	3.5 – 4.0
(Kitagawa and Ohta, 2008)	Numerical: LES	22,000	$1D$	3.25
(Alam, 2014)	Experimental	9,700 – 65,000	–	3.5 – 4.0
(Zhou et al., 2019)	Numerical: LES	1,000	$4D$	3.5 – 4.0
Present study	Numerical: LES	3,000	$4D$	3.75 – 4.0

4.3. Frequency analysis

Strouhal numbers for all spacing ratios $L/D = 1.0 - 5.0$ are grouped in Fig. 12. For $L/D = 1.0 - 1.75$ (small distances) and $L/D = 2.0$ to 3.0, there is a clear difference in the current predictions and experimental data. This is merely due to the high Reynolds number used in the

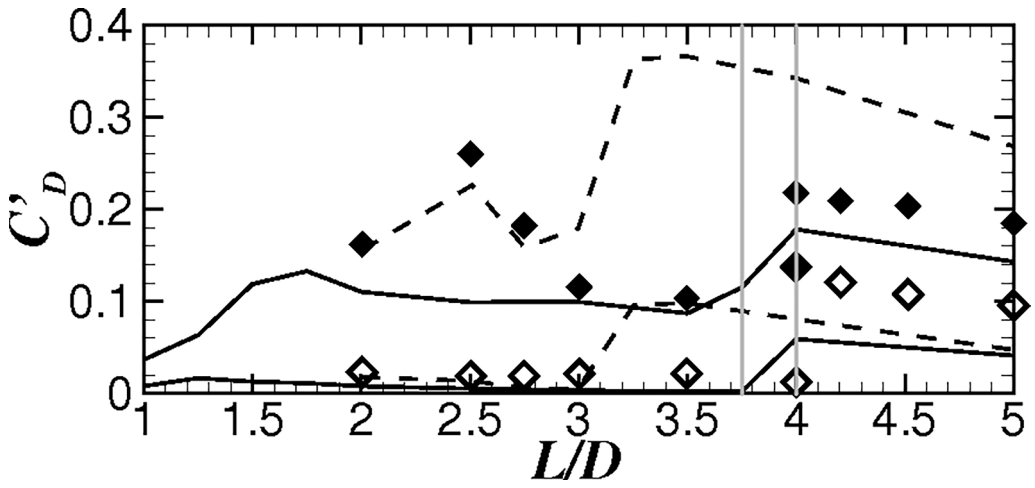

Fig. 7. Variance of the drag coefficient for two cylinders in tandem with various spacing ratios $L/D = 1.0$ to 5.0. Open Symbol: upstream cylinder, full symbol: downstream cylinder. –: LES, — : LES (Kitagawa and Ohta, 2008) $Re = 22,000$, ◊ and ◆: Exp (Moriya et al., 2001) Re = 65, 000.

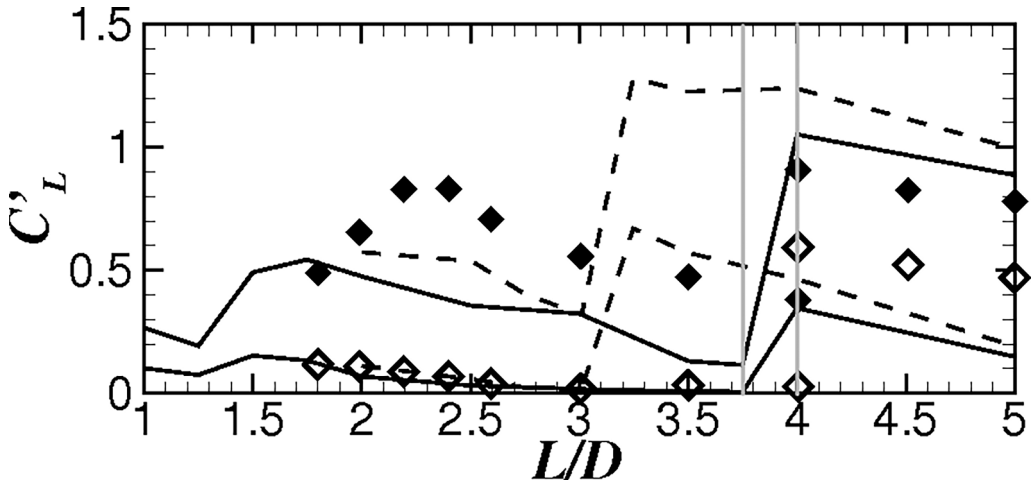

Fig. 8. Variance of the lift coefficient for two cylinders in tandem with various spacing ratios $L/D = 1.0$ to 5.0. Open Symbol: upstream cylinder, full symbol downstream cylinder. –: LES, — : LES (Kitagawa and Ohta, 2008) $Re = 22,000$, ◊ and ◆: Exp (Moriya et al., 2001) $Re = 65,000$.

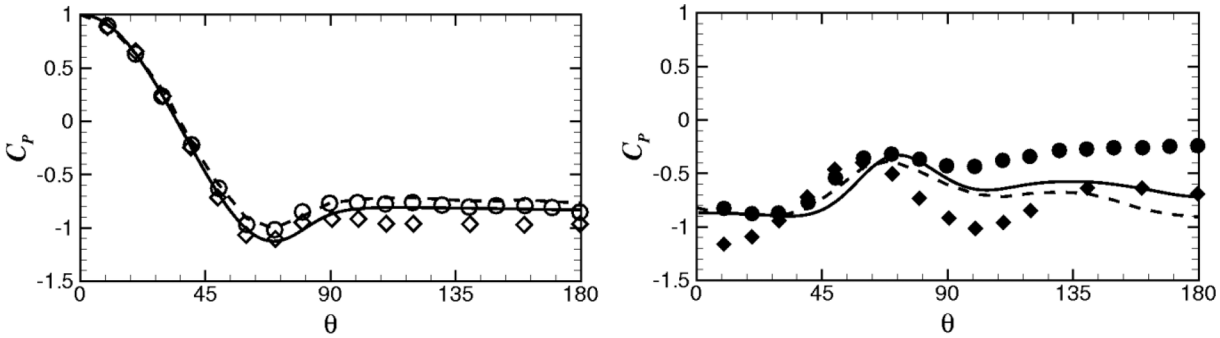

Fig. 9. Mean pressure coefficient for the two cylinders in tandem with ($L/D = 2.0$). Left: upstream cylinder, right: downstream cylinder. –: LES, — : LES (Kitagawa and Ohta, 2008) $Re = 22,000$, ○ and ●: Exp (Ljungkrona et al., 1991) $Re = 20,000$, ◊ and ◆: Exp (Moriya et al., 1983) $Re = 90,000$.

experiments. However, for $L/D > 3.0$, the current predictions coincide perfectly with the experimental and numerical data (downstream cylinder). It remains to note that for cases with spacing $L/D = 3.5$ and 3.75, the values of the Strouhal number do not vary too much compared to other spacing ratios; however, these values decrease until they reach the minimum Strouhal number of 0.15. This is due to the positioning of these two configurations in the critical area where the jump may occur at any time.

Fig. 13 represents energy spectra for lift signals for different spacing ratios $L/D = 1.0$ to 5.0. One sees for the configuration with $L/D = 1.0$ that the behaviour of the two cylinders in tandem is almost identical to that of a single cylinder. This configuration represents the first regime of flows around two cylinders in tandem, as reported earlier.

For the energy spectrum that represents the configuration with the

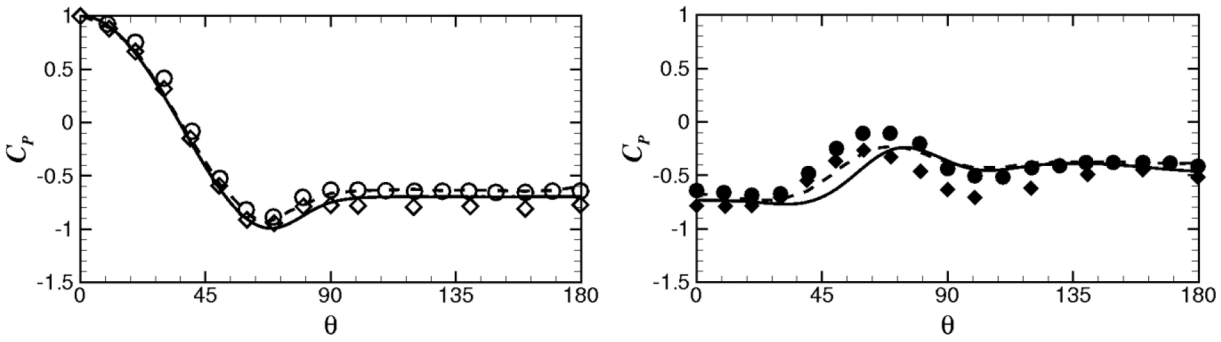

Fig. 10. Mean pressure coefficient for the two cylinders in tandem with ($L/D = 3.0$). Left: upstream cylinder, right: downstream cylinder. –: LES, — : LES (Kitagawa and Ohta, 2008) $Re = 22,000$, ○ and ●: Exp (Ljungkrona et al., 1991) $Re = 20,000$, ◇ and ◆: Exp (Moriya et al., 1983) $Re = 90,000$.

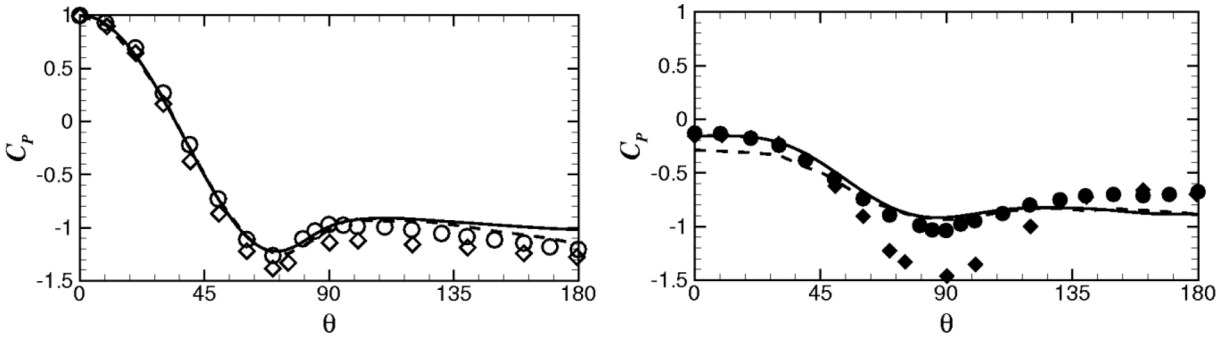

Fig. 11. Medium pressure coefficient for the two cylinders in tandem with ($L/D = 4.0$). Left: upstream cylinder, right: downstream cylinder. –: LES, — : LES (Kitagawa and Ohta, 2008) $Re = 22,000$, ○ and ●: Exp (Ljungkrona et al., 1991) $Re = 20,000$, ◇ and ◆: Exp (Moriya et al., 1983) $Re = 90,000$.

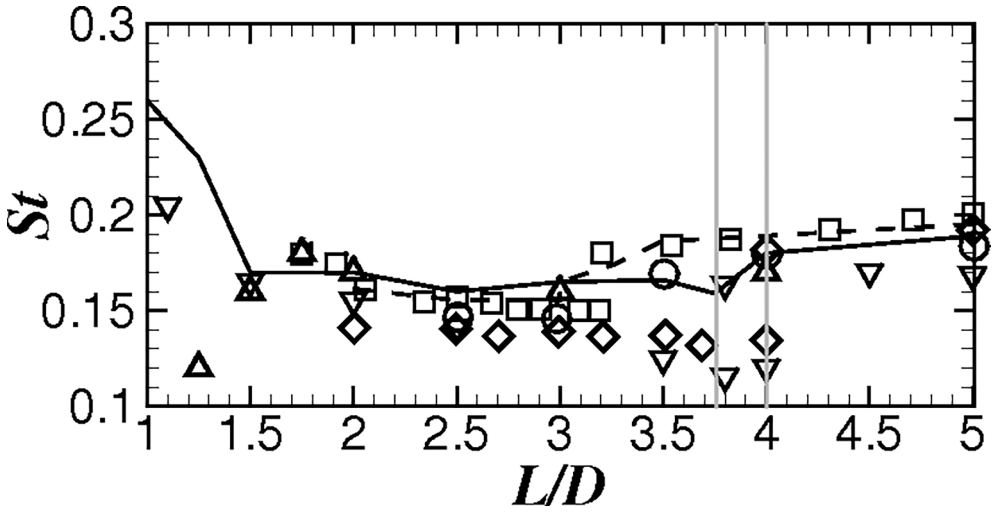

Fig. 12. Strouhal number for various spacing ratios $L/D = 1.0$ to 5.0. –: LES, — : LES (Kitagawa and Ohta, 2008) $Re = 22,000$, ○: Exp (Ljungkrona et al., 1991) $Re = 20,000$, □: Exp (Igarashi, 1981) $Re = 35,000$, ◇: Exp (Moriya et al., 2001) $Re = 65,000$, △: Exp (Alam et al., 2003) $Re = 65,000$, ▽: Exp (Ishigai et al., 1972) $Re = 13,000$.

spacing ratio of $L/D = 1.25$, several peaks (0.177, 0.237, and 0.379) were observed. This shows that the flow is in phase of a mode change (different modes as discussed in the article for the cylinders placed side by side (Afgan et al., 2011)).

Between $L/D = 1.5$ and 2.5 the energy peaks are the same and the Strouhal number is roughly constant at 0.17, this represents the third regime that has been widely studied in the literature.

With spacing ratios of $L/D = 3.0$ to 3.75, one notices the appearance of several energy peaks which vary with the increase in distance between the two cylinders in tandem. This once again shows that a new flow regime is about to change the mode (referred to as a "jump" in the literature).

4.4. Heat transfer

In this section, the heat transfer is discussed for upstream and downstream cylinders according to the spacing ratio and the Prandtl number. To evaluate the effect of the flow field on the heat transfer, the variation of the mean Nusselt number $\langle Nu \rangle$ and the root mean square of its fluctuations $\sqrt{Nu'2}$, normalized by $\sqrt{Re}$, are calculated. In addition,

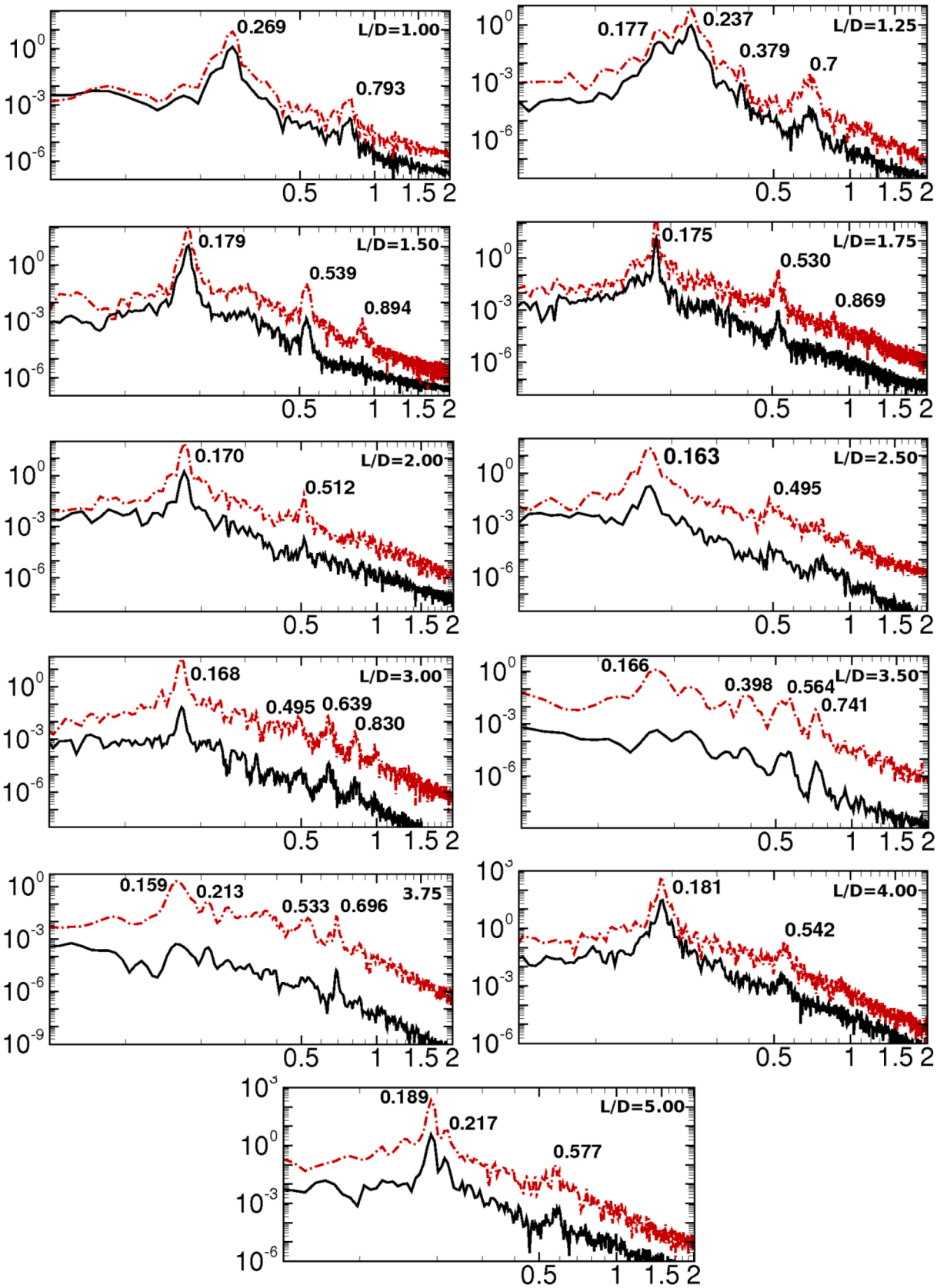

Fig. 13. Energy spectrum of the lift for tandem cylinders with spacing ratios $L/D = 1.0$ to 5.0. Solid black line: Upstream cylinder and dash-dotted red line: downstream cylinder. (For interpretation of the references to colour in this figure legend, the reader is referred to the web version of this article.)

the averaged Nusselt number along the cylinder circumference $\langle Nu \rangle_{avrg}$ is used to compare the global heat transfer for different cases. The symbol $\langle . \rangle$ refers to mean/average in time and the subscript "avrg" refers to averaging along the cylinder circumference θ.

Fig. 14 shows the averaged mean Nusselt number $\langle Nu \rangle_{avrg}$ for different spacing ratios L/D. It shows that for L/D up to 3, the $\langle Nu \rangle_{avrg}$ around the upstream cylinder is higher than that of the downstream cylinder. However, for $L/D \geq 3$, the Nusselt number of the upstream cylinder and downstream cylinder becomes similar. For $L/D = 1$, $\langle Nu \rangle_{avrg}$ of the upstream cylinder is 125% and 76% higher than that of the downstream cylinder for $Pr = 0.1$ and $Pr = 1$, respectively. At the critical spacing $3.75 < L/D \leq 4.0$, a drastic variation occurs for $\langle Nu \rangle_{avrg}$ of both cylinders (22% and 40% for $Pr = 0.1$ and $Pr = 1$, respectively). This variation occurs at the same critical spacing as the "jumping" for the flow structures. For all L/D ratios, $\langle Nu \rangle_{avrg}$ increases with increasing Prandtl number.

The local mean Nusselt number $\langle Nu \rangle$ and its root mean square ($\sqrt{Nu'2}$) on the cylinder surfaces are illustrated in Figs. 15 to 18 for the two Prandtl number ($Pr = 0.1$ and $Pr = 1$). The development of the boundary layer on the heated cylinders, its separation, and the vortex shedding, all together affect the variation of the Nusselt number on the cylinder surface. Moreover, the Nusselt number on the downstream cylinder is governed by the wake behaviour of the upstream one.

4.4.1. *Upstream cylinder:*

For all cases, $\langle Nu \rangle$ on the upstream cylinder surface is maximum near the front stagnation point ($\theta \approx 0^0$) where the boundary layer is very thin. It decreases along the front side of the cylinder until the separation point ($85^0 \leq \theta \leq 90^0$) due to the development of the boundary layer which increases the thermal resistance. It is worth mentioning that the presence of the downstream cylinder does not affect the heat transfer along the front side of the upstream one. For $L/D = 1$ and 1.25, $\langle Nu \rangle$ keeps decreasing on the back side of the cylinder until it vanishes at the rear stagnation point $\theta \approx 180^0$. For $1.5 \leq L/D \leq 2.0$, $\langle Nu \rangle$ increases slowly, whereas it remains constant on the back side for $L/D > 2$.

Regarding the fluctuations, $\sqrt{\langle Nu'2 \rangle}$ has a very low value along the front side of the cylinder and before the separation which can be explained by the laminar flow regime at the front side of the cylinder. However, after separation, $\sqrt{\langle Nu'2 \rangle}$ increases starting from the separation point due to the growth of a turbulent boundary layer. The behaviour of the fluctuating Nusselt number depends on the spacing ratio and the Prandtl number. For $L/D = 1$ and 1.25, the maximum is located at ($\theta \approx 130^0$), while for $L/D > 1.25$, it increases monotonically until the rear stagnation point ($\theta \approx 180^0$).

4.4.2. *Downstream cylinder:*

The heat transfer on the downstream cylinder is affected by the impingement of vortices detached from the upstream cylinder and its behaviour differs from that of the upstream one. The mean Nusselt number does not follow a monotonic trend and different segments can be identified. The maximum value of $\langle Nu \rangle$ is near the impingement location $60^0 \leq \theta_{imp} \leq 80^0$ while its minimum value is at the front stagnation point $\theta \approx 0^0$. For $L/D = 1$ and 1.25, $\langle Nu \rangle$ is very small (≈ 0) because of no vortices at the small gap between the two cylinders which behave as a single extended body. The mean Nusselt number on the downstream cylinder behaves similarly to the pressure coefficient (Figs. 9-11). The attached flow around the downstream cylinder (after the impingement location and before re-separation $116 \leq \theta_{sep} \leq 125^0$) results in the formation of an attached boundary layer which increases the thermal resistance and hence decreases the Nusselt number. The re-attachment zone situated between the impingement and re-separation ($\theta_{imp} \leq \theta \leq \theta_{sep}$) increases with increasing spacing ratios. In fact, increasing the spacing ratio decreases the impingement location and delays the re-separation. After separation, $\langle Nu \rangle$ increases again due to the flow transition to turbulence, thereby, enhancing the fluid mixing. The Nusselt number variation can be divided into three different regions (Dhiman et al., 2017b; Zafar and Alam, 2018): (i) impingement zone for $0 \leq \theta \leq \theta_{imp}$ with increasing $\langle Nu \rangle$, re-attachment zone for $\theta_{imp} \leq \theta \leq \theta_{sep}$ with decreasing $\langle Nu \rangle$, and turbulent recirculation zone for $\theta_{sep} \leq \theta \leq 180^0$ with increasing $\langle Nu \rangle$. The minimum (at $\theta \approx 0^0$) and the maximum value of $\langle Nu \rangle$ increases by increasing the spacing ratios and the Prandtl number.

In general, the fluctuations follow the behaviour of the mean Nusselt number. Similar to $\langle Nu \rangle$, $\sqrt{\langle Nu'2 \rangle}$ is minimum at the front stagnation point $\theta \approx 0^0$ for all cases. However, its maximum is located at the rear stagnation point $\theta \approx 180^0$ for the extended body regime ($L/D = 1$ and 1.25) and it is located at the impingement position (θ_{imp}) for all other cases. It is important to mention here that the fluctuations follow the behaviour of the mean Nusselt number.

5. Conclusions

The flow and heat transfer around two tandem cylinders were investigated using Large Eddy Simulations at subcritical Reynolds

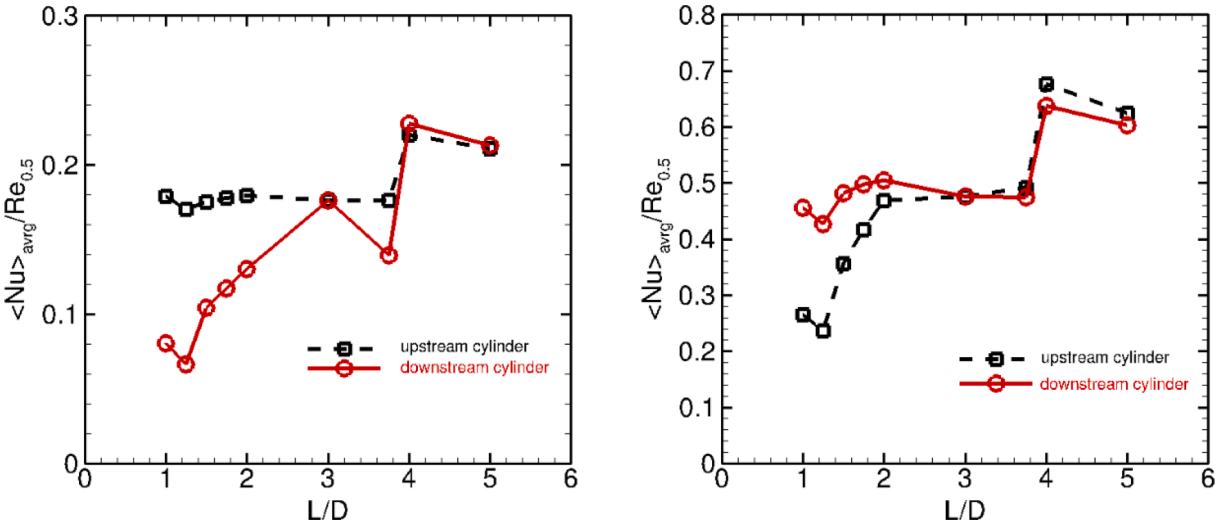

Fig. 14. Averaged (along θ) mean Nusselt number for different spacing ratios L/D: dashed line for upstream cylinder and solid line for the downstream cylinder. Prandtl number (left) $Pr = 0.1$ and (right) $Pr = 1$.

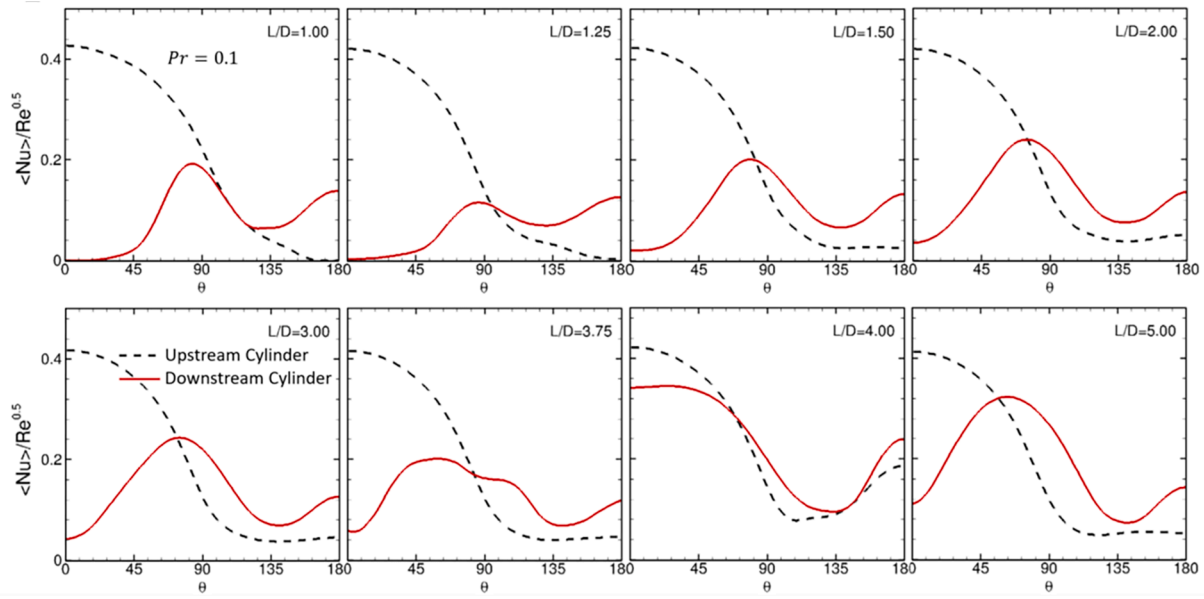

Fig. 15. Prandtl number $Pr = 0.1$: mean normalized Nusselt number, $< Nu > /Re^{0.5}$ around the tandem cylinders with spacing ratios $L/D = 1.0$ to 5.0.

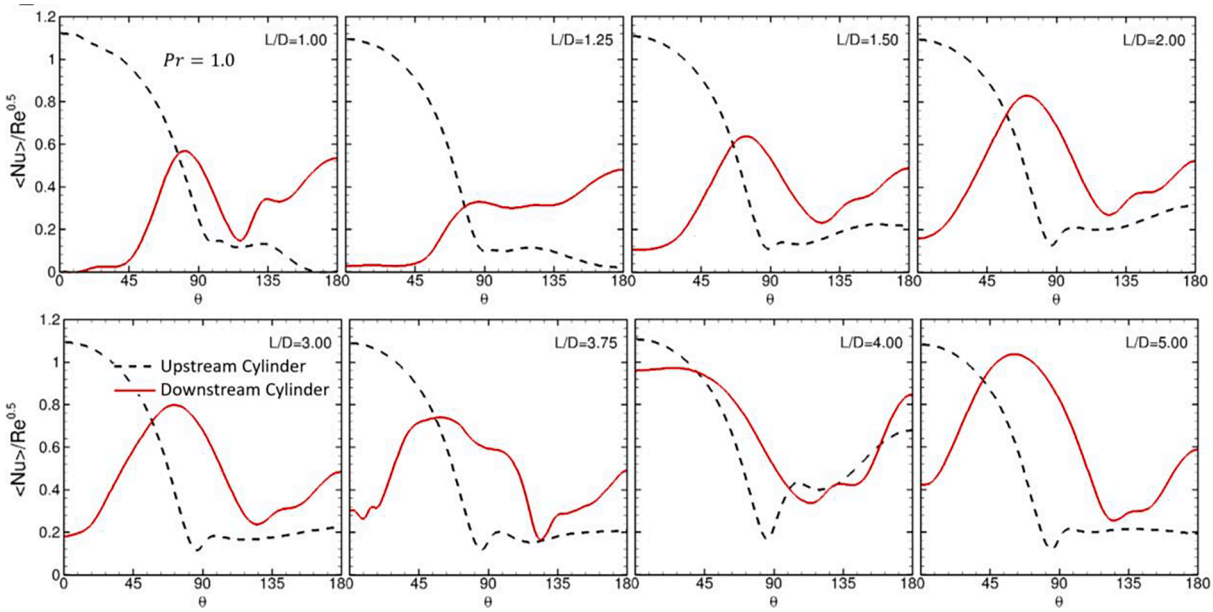

Fig. 16. Prandtl number $Pr = 1.0$: mean normalized Nusselt number, $< Nu > /Re^{0.5}$ around the tandem cylinders with spacing ratios $L/D = 1.0$ to 5.0.

number $Re = 3{,}000$. The spacing ratio between the cylinder centers was varied in increments of 0.25 over the range $1.0 \leq L/D \leq 5.0$. Two different Prandtl numbers were considered $Pr = 0.1$ and 1.0. Special attention was paid to the zones of vortex formation to understand the physics of the flow for this kind of configuration.

Results showed that the flow structures vary according to the spacing ratio. Three main flow regimes were identified (extended-body regime, reattachment regime and co-shedding regime) which were all found to be in good agreement with literature. For low spacing ratios ($1.0 \leq L/D \leq 1.25$), flow regime without reattachment of the shear layer is established and the cylinders behave as a single body with vortex shedding behind the downstream cylinder. For spacing ratio ($1.5 \leq L/D \leq 3.75$), the shear layer separated from the upstream cylinder reattaches the downstream cylinder, hence the name reattachment regime. This regime can be categorized into multiple sub-regimes depending upon either the reattachment location on the downstream cylinder ("after-body" or "fore-body" reattachment regime) or the vortex shedding of the downstream cylinder (without vortex shedding for $1.5 \leq L/D \leq 2.0$) and with vortex shedding for $2.0 \leq L/D \leq 3.75$). For the higher spacing ratio ($4.0 \leq L/D \leq 5.0$); co-shedding regime, the two cylinders behave as separated single cylinders and vortex shedding is established behind both cylinders. The change of flow regime "jump" occurs at a critical spacing ratio of $(L/D)_{cr} = 3.75$, which is in good agreement with experimental and numerical data available in literature.

It was found that the lift and drag fluctuations on the downstream cylinder were very sensitive to the spacing ratios between the cylinders, especially before the critical step. However, after the critical step ($L/D = 3.75$ and 4.0) they remained more or less constant. The values of the Strouhal number also vary with the variation of the spacing between the two cylinders.

The heat transfer analysis showed that for L/D up to 3 the averaged Nusselt number along the upstream cylinder is higher than that along

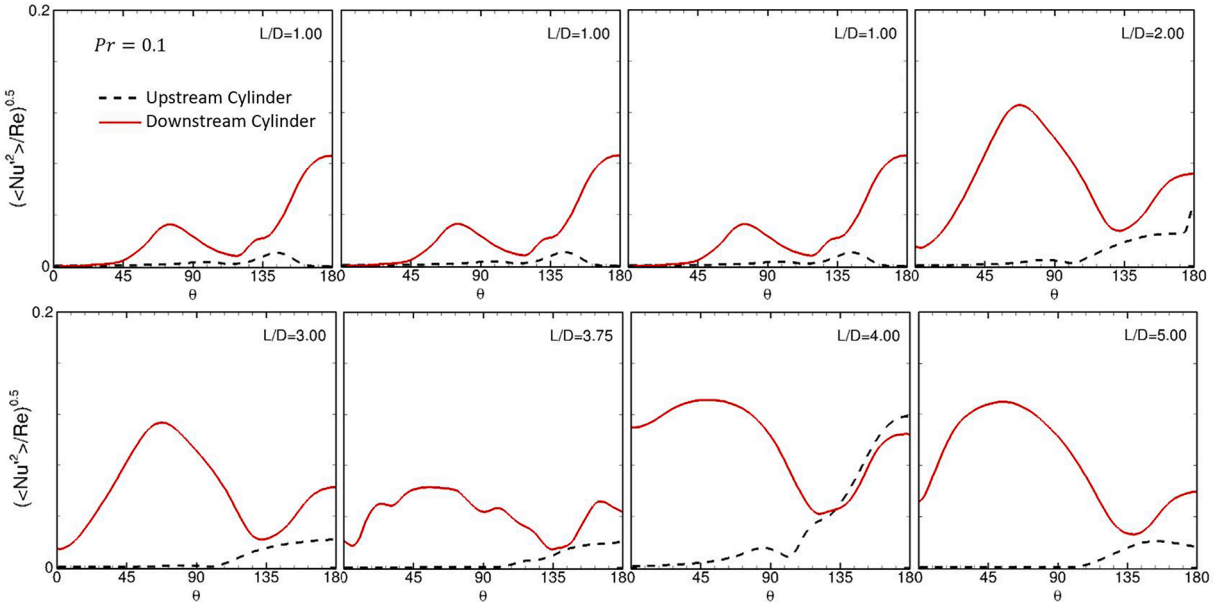

Fig. 17. Prandtl number $Pr = 0.1$: fluctuating normalized Nusselt number, $\left(\langle Nu'^2 \rangle / Re\right)^{0.5}$ around the tandem cylinders with spacing ratios $L/D = 1.0$ to 5.0.

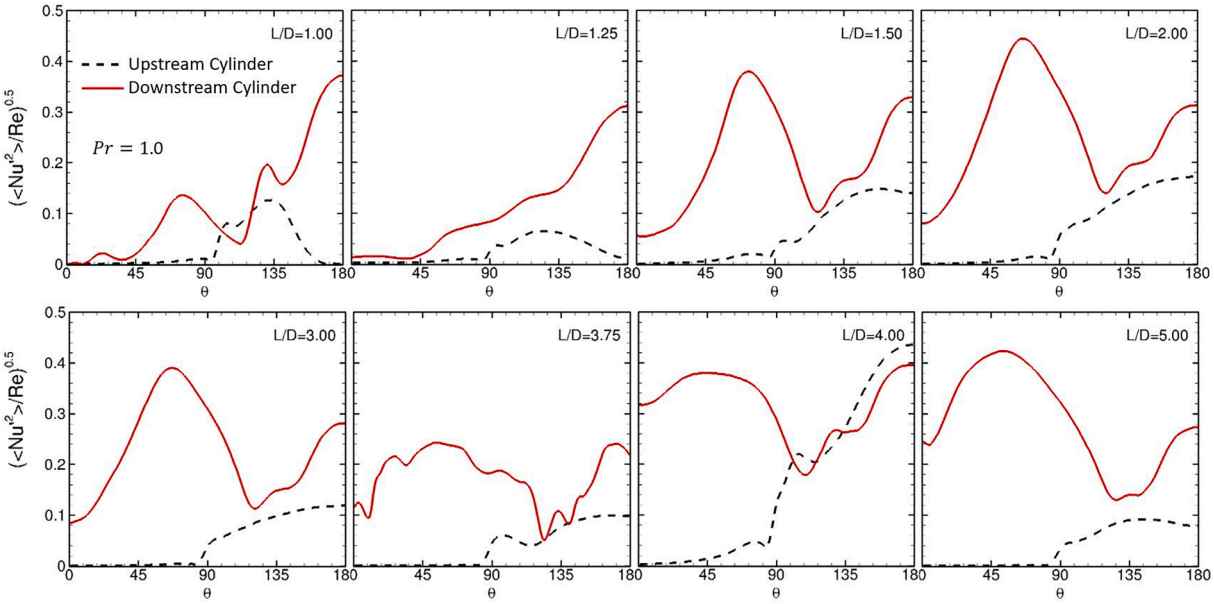

Fig. 18. Prandtl number $Pr = 1.0$: fluctuating normalized Nusselt number, $\left(\langle Nu'^2 \rangle / Re\right)^{0.5}$ around the tandem cylinders with spacing ratios $L/D = 1.0$ to 5.0.

the downstream cylinder. For higher spacing ratios, the Nusselt number is similar for both the cylinders. Furthermore, a drastic variation of the Nusselt number occurs at a critical spacing ratio corresponding to the "jumping" on the wake topology of the tandem cylinders. The overall Nusselt number (sum of the two cylinders) increases with increasing the spacing ratio. Moreover, a significant increase in the overall Nusselt number is reached at the critical spacing ratio. The Nusselt number variation along the downstream cylinder's circumference can be divided into three regions: impingement region, re-attachment region, and turbulent recirculation region.

Declaration of Competing Interest

The authors declare that they have no known competing financial interests or personal relationships that could have appeared to influence the work reported in this paper.

Data availability

Data will be made available on request.

Acknowledgments

The authors thank the support provided by the UAE Ministry of Education (CRPG-2019, Grant No. 1570604539) and the Emirates Nuclear Technology Center (ENTC), Khalifa University of Science and Technology, UAE. The authors are thankful to Électricité de France (EDF) for providing the computational resources.

References

Abed, N., Afgan, I., 2017. A CFD study of flow quantities and heat transfer by changing a vertical to diameter ratio and horizontal to diameter ratio in inline tube banks using URANS turbulence models. Int. Commun. Heat Mass Transf. 89, 18–30. https://doi.org/10.1016/j.icheatmasstransfer.2017.09.015.

Abed, N., Afgan, I., Cioncolini, A., Iacovides, H., Nasser, A., 2020a. Assessment and Evaluation of the Thermal Performance of VariousWorking Fluids in Parabolic Trough Collectors of Solar Thermal Power Plants under Non-Uniform Heat Flux Distribution Conditions. Energies 13 (15), 3776.

Abed, N., Afgan, I., Cioncolini, A., Iacovides, H., Nasser, A., Mekhail, T., 2020b. Thermal performance evaluation of various nanofluids with non-uniform heating for parabolic trough collectors. Case Stud. Therm. Eng. 22, 100769 https://doi.org/10.1016/j.csite.2020.100769.

Abed, N., Afgan, I., Nasser, A., Iacovides, H., Cioncolini, A., Mekhail, T., 2020c. Numerical Investigations of parabolic trough collectors using different nanofluids. Int. J. Appl. Energy Syst. 2, 88–94. https://doi.org/10.21608/ijaes.2020.169898.

Abed, N., Afgan, I., Iacovides, H., Cioncolini, A., Khurshid, I., Nasser, A., 2021. Thermal-hydraulic analysis of parabolic trough collectors using straight conical strip inserts with nanofluids. Nanomaterials 11 (4), 853.

Adobes, A., Jusserand, F., Benhamadouche, S., Kahil, Y., Belouah, S., Computation of Fluid Forces Acting on an Infinite Cylinder Submitted to a Single Phase Cross Flow. Proceedings of the ASME 2010 3rd Joint US-European Fluids Engineering Summer Meeting collocated with 8th International Conference on Nanochannels, Microchannels, and Minichannels. ASME 2010 7th International Symposium on Fluid-Structure Interactions, Flow-Sound Interactions, and Flow-Induced Vibration and Noise: Volume 3, Parts A and B. Montreal, Quebec, Canada. August 1–5, 2010. pp. 241-250. ASME. https://doi.org/10.1115/FEDSM-ICNMM2010-30016.

Afgan, I., Moulinec, C., Laurence, D., 2008. Numerical simulation of generic side mirror of a car using large eddy simulation with polyhedral meshes. Int. J. Numer. Methods Fluids 56, 1107–1113. https://doi.org/10.1002/fld.1719.

Afgan, I., Kahil, Y., Benhamadouche, S., Sagaut, P., 2011. Large eddy simulation of the flow around single and two side-by-side cylinders at subcritical Reynolds numbers. Phys. Fluids 23, 1–17. https://doi.org/10.1063/1.3596267.

Afgan, I., 2007. Large Eddy Simulation of Cylindrical Bodies Incorporating Unstructured Finite Volume Mesh. A thesis submitted to The University of Manchester for the degree of Doctor of Philosophy in the Faculty of Engineering and Physical Sciences.

Ahmed, U., Apsley, D., Stallard, T., Stansby, P., Afgan, I., 2021. Turbulent length scales and budgets of Reynolds stress-transport for open-channel flows; friction Reynolds numbers R eτ = 150, 400 and 1020. J. Hydraul. Res. 59, 36–50. https://doi.org/10.1080/00221686.2020.1729265.

Alam, M.M., 2014. The aerodynamics of a cylinder submerged in the wake of another. J. Fluids Struct. 51, 393–400. https://doi.org/10.1016/j.jfluidstructs.2014.08.003.

Alam, M.M., 2016. Lift forces induced by phase lag between the vortex sheddings from two tandem bluff bodies. J. Fluids Struct. 65, 217–237. https://doi.org/10.1016/j.jfluidstructs.2016.05.008.

Alam, M.M., Moriya, M., Takai, K., Sakamoto, H., 2003. Fluctuating fluid forces acting on two circular cylinders in a tandem arrangement at a subcritical Reynolds number. J. Wind Eng. Ind. Aerodyn. 91, 139–154. https://doi.org/10.1016/S0167-6105(02)00341-0.

Alameri, S.A., Alkaabi, A.K., 2020. Fundamentals of nuclear reactors. In: Nuclear Reactor Technology Development and Utilization. Woodhead Publishing, pp. 27–60.

Ali, A., Afgan, I., Laurence, D., Revell, A., 2021a. A dual-mesh hybrid RANS-LES simulation of the buoyant flow in a differentially heated square cavity with an improved resolution criterion. Comput. Fluids 224, 104949. https://doi.org/10.1016/j.compfluid.2021.104949.

Ali, A., Afgan, I., Laurence, D., Revell, A., 2022. A dual-mesh hybrid Reynolds-averaged Navier-Stokes/Large eddy simulation study of the buoyant flow between coaxial cylinders. Nucl. Eng. Des. 393, 111789 https://doi.org/10.1016/j.nucengdes.2022.111789.

Ali, U., Janajreh, I., Fatt, Y., Alam, M., 2021b. Flow-Induced Vibrations of Single and Multiple Heated Circular Cylinders : A Review. Energies 14. https://doi.org/10.3390/en14248496.

Archambeau, F., Méchitoua, N., Sakiz, M., 2004. Code Saturne: A Finite Volume Code for Turbulent flows - Industrial Applications. Int. J. Finite 1.

Benhamadouche, S., 2006. Large eddy simulation with the unstructured collocated arrangement. University of Manchester. PhD Thesis.

Benhamadouche, S., Afgan, I., Manceau, R., 2020. Numerical Simulations of Flow and Heat Transfer in a Wall-Bounded Pin Matrix. Flow. Turbul. Combust. 104, 19–44. https://doi.org/10.1007/s10494-019-00046-8.

Benhamadouche, S., Laurence, D., Jarrin, N., Afgan, I. 2005. Large Eddy Simulation of flow across in-line tube bundles. NURETH 11, Avignon, Fracne, 2-6 October 2005.

Carmo, B.S., Meneghini, J.R., Sherwin, S.J., 2010a. Possible states in the flow around two circular cylinders in tandem with separations in the vicinity of the drag inversion spacing. Phys. Fluids 22, 1–7. https://doi.org/10.1063/1.3420111.

Carmo, B.S., Meneghini, J.R., Sherwin, S.J., 2010b. Secondary instabilities in the flow around two circular cylinders in tandem. J. Fluid Mech. 644, 395–431. https://doi.org/10.1017/S0022112009992473.

Dehkordi, B.G., Moghaddam, H.S., Jafari, H.H., 2011. Numerical simulation of flow over two circular cylinders in tandem arrangement. J. Hydrodyn. 23, 114–126. https://doi.org/10.1016/S1001-6058(10)60095-9.

Dhiman, S.K., Kumar, A., Prasad, J.K., 2017a. Unsteady computation of flow field and convective heat transfer over tandem cylinders at subcritical Reynolds numbers. J. Mech. Sci. Technol. 31, 1241–1257. https://doi.org/10.1007/s12206-017-0223-0.

Dhiman, S.K., Prasad, J.K., Kumar, A., 2017b. Unsteady convective heat transfer in cross flow past two tandem cylinders: an inverse heat conduction approach. Heat Mass Transf. und Stoffuebertragung 53, 1761–1775. https://doi.org/10.1007/s00231-016-1927-x.

Ferziger, J.H., Perić, M. (Eds.), 2002. Computational Methods for Fluid Dynamics. Springer Berlin Heidelberg, Berlin, Heidelberg.

Filippone, A., Afgan, I., 2008. Orthogonal blade-vortex interaction on a helicopter tail rotor. AIAA J. 46, 1476–1489. https://doi.org/10.2514/1.32690.

Germano, M., Piomelli, U., Moin, P., Cabot, W.H., 1991. A dynamic subgrid-scale eddy viscosity model. Phys. Fluids A 3, 1760–1765. https://doi.org/10.1063/1.857955.

Guleren, K.M., Afgan, I., Turan, A., 2010. Predictions of turbulent flow for the impeller of a NASA low-speed centrifugal compressor. J. Turbomach. 132, 021005 https://doi.org/10.1115/1.3140824.

Han, X., Sagaut, P., Lucor, D., Afgan, I., 2012. Stochastic response of the laminar flow past a flat plate under uncertain inflow conditions. International Journal of Computational Fluid Dynamics 26 (2), 101–117.

Harimi, I., Saghafian, M., 2012. Numerical simulation of fluid flow and forced convection heat transfer from tandem circular cylinders using overset grid method. J. Fluids Struct. 28, 309–327. https://doi.org/10.1016/j.jfluidstructs.2011.12.006.

Huhe-Aode, H., Tatsuno, M., Taneda, S., 1985. Visual studies of wake structure behind two cylinders in tandem arrangement, Kyushu University, Japan, Report No. 32(99).

Igarashi, T., 1981. Characteristics of the flow around two circular cylinders arranged in tandem (1st report). Bull. JSME 24 (188), 323–331.

Igarashi, T., 1984. Characteristics of the flow around two circular cylinders arranged in tandem (2st report). Bull. JSME 27, 233–242. https://doi.org/10.1299/jsme1958.27.2380.

Ishigai, S., Nishikawa, E., Nishimura, K., Cho, K., 1972. Experimental study on structure of gas flow in tube banks with tube axis normal to flow. Bull. JSME 15, 949–956.

Jester, W., Kallinderis, Y., 2003. Numerical study of incompressible flow about fixed cylinder pairs. J. Fluids Struct. 17, 561–577. https://doi.org/10.1016/S0889-9746(02)00149-4.

Kahil, Y., Benhamadouche, S., Berrouk, A.S., Afgan, I., 2019. Simulation of subcritical-Reynolds-number flow around four cylinders in square arrangement configuration using LES. Eur. J. Mech. B/Fluids 74, 111–122. https://doi.org/10.1016/j.euromechflu.2018.11.008.

Kim, J.H., Song, M.M., Alameri, S.A., 2019. Emerging areas of nuclear power applications. Nuclear Engineering and Design 354, 110183.

Kitagawa, T., Ohta, H., 2008. Numerical investigation on flow around circular cylinders in tandem arrangement at a subcritical Reynolds number. J. Fluids Struct. 24, 680–699. https://doi.org/10.1016/j.jfluidstructs.2007.10.010.

Koda, Y., Lien, F.S., 2013. Aerodynamic effects of the early three-dimensional instabilities in the flow over one and two circular cylinders in tandem predicted by the lattice Boltzmann method. Comput. Fluids 74, 32–43. https://doi.org/10.1016/j.compfluid.2013.01.003.

Lilly, D.K., 1992. A proposed modification of the Germano subgrid-scale closure method. Phys. Fluids A 4, 633–635. https://doi.org/10.1063/1.858280.

Ljungkrona, L., Norberg, C., Sundén, B., 1991. Free-stream turbulence and tube spacing effects on surface pressure fluctuations for two tubes in an in-line arrangement. J. Fluids Struct. 5, 701–727. https://doi.org/10.1016/0889-9746(91)90364-U.

Ljungkrona, L., Sundén, B., 1993. Flow visualization and surface pressure measurement on two tubes in an inline arrangement. Exp. Therm. Fluid Sci. 6, 15–27. https://doi.org/10.1016/0894-1777(93)90037-J.

Lockard, D.P., 2011. Summary of the tandem cylinder solutions from the benchmark problems for airframe noise computations-I workshop. In: 49th AIAA Aerosp Sci. Meet. Incl. New Horizons Forum Aerosp. Expo., pp. 1–22. https://doi.org/10.2514/6.2011-353.

Maduta, R., Ullrich, M., Jakirlic, S., 2017. Reynolds stress modelling of wake interference of two cylinders in tandem: Conventional vs. eddy-resolving closure. Int. J. Heat Fluid Flow 67, 139–148. https://doi.org/10.1016/j.ijheatfluidflow.2017.07.012.

Mahír, N., Altaç, Z., 2008. Numerical investigation of convective heat transfer in unsteady flow past two cylinders in tandem arrangements. Int. J. Heat Fluid Flow 29, 1309–1318. https://doi.org/10.1016/j.ijheatfluidflow.2008.05.001.

Mittal, S., Kumar, V., Raghuvanshi, A., 1997. Unsteady incompressible flows past two cylinders in tandem and staggered arrangements. Int. J. Numer. Methods Fluids 25, 1315–1344. https://doi.org/10.1002/(sici)1097-0363(19971215)25:11<1315::aid-fld617>3.0.co;2-p.

Moriya, M., Sakamoto, H., Kiya, M., Arie, M., 1983. Fluctuating pressures and forces on two circular cylinders in tandem arrangement. Trans. JSME 49 (443), 1364–1372.

Moriya, M., Alam, M.M., Takai, K., Sakamoto, H., Matsumoto, M., Shirato, H., Araki, K., Haramura, T., Hashimoto, T., Kobayashi, H., Okumura, M., Matsutani, Y., Park, C.-W., Lee, S.-J., Luo, S.C., Khoo, B.C., Tong, X.H., Ohya, Y., Watanabe, K., Li, Y.F., Flay, R.G.J., Richards, P.J., 2001. Fluctuating Fluid Forces Acting on Two Circular Cylinders in a Tandem Arrangement at a Subcritical Reynolds Number. J Wind Eng. 2001 (89), 697–724.

Nguyen, P.T.L., Uribe, J.C., Afgan, I., Laurence, D.R., 2020. A Dual-Grid Hybrid RANS/LES Model for Under-Resolved Near-Wall Regions and its Application to Heated and Separating Flows. Flow. Turbul. Combust. 104, 835–859. https://doi.org/10.1007/s10494-019-00070-8.

Papaioannou, G.V., Yue, D.K.P., Triantafyllou, M.S., Karniadakis, G.E., 2006. Three-dimensionality effects in flow around two tandem cylinders. J. Fluid Mech. 558, 387–413. https://doi.org/10.1017/S0022112006000139.

Parezanović, V., Cadot, O., 2012. Experimental sensitivity analysis of the global properties of a two-dimensional turbulent wake. Journal of Fluid Mechanics 693, 115–149.

Parezanović, V., Monchaux, R., Cadot, O., 2015. Characterization of the turbulent bistable flow regime of a 2D bluff body wake disturbed by a small control cylinder. Experiments in Fluids 56 (1), 1–8.

Parnaudeau, P., Carlier, J., Heitz, D., Lamballais, E., 2008. Experimental and numerical studies of the flow over a circular cylinder at Reynolds number 3900. Phys. Fluids 20, 1–14. https://doi.org/10.1063/1.2957018.
Rastan, M.R., Alam, M.M., 2021. Transition of wake flows past two circular or square cylinders in tandem. Phys. Fluids 33 (8), 081705.
Revell, A., Afgan, I., Ali, A., Santasmasas, M., Craft, T., Rosis, A. de, Holgate, J., Laurence, D., Iyamabo, B., Mole, A., Owen, B., Savoie, M., Skillen, A., Wang, J., Zhang, X., 2020. Coupled Hybrid RANS-LES Research at The University of Manchester. ERCOFTAC Bull. Eur. Res. Community Flow, Turbul. Combust. 2020, Prog. RANS-based Scale-Resolving Flow Simul. Methods 120, 67.
Rhie, C., Chow, W., 1983. A numerical study of the flow past an isolated airfoil with trailing edge separation. AIAA J. 21, 1525.
Salcedo, E., Cajas, J.C., Treviño, C., Martínez-Suástegui, L., 2016. Unsteady mixed convection heat transfer from two confined isothermal circular cylinders in tandem: Buoyancy and tube spacing effects. Int. J. Heat Fluid Flow 60, 12–30. https://doi.org/10.1016/j.ijheatfluidflow.2016.04.001.
Sumner, D., 2010. Two circular cylinders in cross-flow: A review. J. Fluids Struct. 26, 849–899. https://doi.org/10.1016/j.jfluidstructs.2010.07.001.
Wong, C.W., Zhou, Y., Alam, M.M., Zhou, T.M., 2014. Dependence of flow classification on the Reynolds number for a two-cylinder wake. J. Fluids Struct. 49, 485–497. https://doi.org/10.1016/j.jfluidstructs.2014.05.008.
Wu, Z., Laurence, D., Afgan, I., 2017. Direct numerical simulation of a low momentum round jet in channel crossflow. Nucl. Eng. Des. 313, 273–284. https://doi.org/10.1016/j.nucengdes.2016.12.018.
Xu, G., Zhou, Y., 2004. Strouhal numbers in the wake of two inline cylinders. Experiments in Fluids 37 (2), 248–256.
Zafar, F., Alam, M.M., 2018. A low Reynolds number flow and heat transfer topology of a cylinder in a wake. Phys. Fluids 30 (8), 083603.
Zafar, F., Alam, M.M., 2020. Mixed convection heat transfer from a circular cylinder submerged in wake. Int. J. Mech. Sci. 183, 105733.
Zdravkovich, M.M., 1987. The effects of interference between circular cylinders in cross flow. J. Fluids Struct. 1, 239–261. https://doi.org/10.1016/S0889-9746(87)90355-0.
Zdravkovich, M.M., 2003. Flow Around Circular Cylinders, Volume 2:. Applications. Oxford University Press, USA.
Zdravkovich, M.M., 1977. Flow Around Circular Cylinders Volume 1: Fundamentals. Oxford Science Publications.
Zhou, Q., Alam, M.M., Cao, S., Liao, H., Li, M., 2019. Numerical study of wake and aerodynamic forces on two tandem circular cylinders at Re = 103. Phys. Fluids 31 (4), 045103.
Zhou, Y., Yiu, M.W., 2006. Flow structure, momentum and heat transport in a two-tandem-cylinder wake. Journal of Fluid Mechanics 548, 17–48.
Iacovides, H., Launder, B. and West, A., 2014. A comparison and assessment of approaches for modelling flow over in-line tube banks. *International journal of heat and fluid flow*, *49*, pp.69-79.